

# Non-equilibrium excitation of methanol in Galactic molecular clouds: multi-transitional observations at 2 mm.

V. I. Slysh, S. V. Kalenskii, I. E. Val'tts, and V. V. Golubev

Astro Space Center, Lebedev Physical Institute, Profsoyuznaya str. 84/32, 117810, Moscow, Russia; vslysh@dpc.asc.rssi.ru, kalensky@dpc.asc.rssi.ru, ivaltts@dpc.asc.rssi.ru, golubev@dpc.asc.rssi.ru

and

K. Mead

National Radio Astronomy Observatory, Arizona Operations, Campus Building 65, 949 N. Cherry Avenue, Tucson, AZ 85721-0665; kmead@nrao.edu

Received \_\_\_\_\_; accepted \_\_\_\_\_

## ABSTRACT

We observed 14 methanol transitions near  $\lambda = 2$  mm in Galactic star-forming regions. Broad, quasi-thermal  $J_0 - J_{-1}E$  methanol lines near 157 GHz were detected toward 73 sources. Together with the  $6_{-1} - 5_0E$  and  $5_{-2} - 6_{-1}E$  lines at 133 GHz and the  $7_1 - 7_0E$  line at 165 GHz, they were used to study the methanol excitation. In the majority of the observed objects, the Class I  $6_{-1} - 5_0E$  transition is inverted, and the Class II  $5_{-2} - 6_{-1}E$  and  $6_0 - 6_{-1}E$  transitions are overcooled. This is exactly as predicted by models of low gain Class I masers. The absence of the inversion of Class II transitions  $5_{-2} - 6_{-1}E$  and  $6_0 - 6_{-1}E$  means that quasi-thermal methanol emission in all objects arises in areas without a strong radiation field, which is required for the inversion.

*Subject headings:* ISM:clouds – ISM:molecules – radio lines:ISM

## 1. Introduction

Methanol in space has been intensively studied since its discovery (Ball et al. 1970). Most of the attention has been concentrated on methanol masers, and much less effort has been put into studies of thermal methanol. The methanol molecule is a slightly asymmetric top with hindered internal rotation, and possesses a large number of allowed transitions at radio frequencies. Multi-transitional observations can be used to determine the main properties of the ambient gas—temperature and density—and of the methanol itself (column density and abundance; Menten et al. 1988; Kalenskii et al. 1997).

Ziurys & McGonagle (1993) detected a series of  $J_0 - J_{-1}E$  lines near 157 GHz toward Ori-KL. Observations in these lines have an additional advantage that, because they can be observed simultaneously with the same receiver, their relative intensities are free from calibration errors. We made an extensive survey of galactic star-forming regions in these lines. In addition, most sources were observed in the  $6_{-1} - 5_0E$ ,  $6_2 - 7_1A^-$ , and  $5_{-2} - 6_{-1}E$  lines near 133 GHz and six objects were observed in the  $7_1 - 7_0E$  line near 166 GHz. According to statistical equilibrium (SE) calculations, both thermal and maser emission are possible in all these lines.

## 2. Observations

All lines were observed with the 12-m NRAO <sup>1</sup> telescope at Kitt Peak, AZ. The observations at 157 GHz were made in March 1994. The receiver setup and observing mode was described in Slysh et al. (1995). A hybrid spectrometer with 150 MHz total bandwidth and 768 channels was used, providing frequency resolution of 195 kHz ( $0.37 \text{ km s}^{-1}$ ); the bandwidth of the spectrometer allowed us to observe the  $J = 1 - 5$  lines simultaneously. Many sources were also observed with a 256-channel filter spectrometer with 2 MHz resolution, operating in parallel with the

---

<sup>1</sup>NRAO is operated by Associated Universities, Inc., under contract with the National Science Foundation.

hybrid spectrometer; the bandwidth of the spectrometer allowed us to observe simultaneously the  $J = 1 - 6$  lines. Eight  $J_0 - J_{-1}E$  methanol lines were observed in W3(OH), 345.01+1.79, W48 and Cep A by tuning the receiver to appropriate frequencies.

The observations at 133 GHz were made on June 5–7, 1995, and the observations at 166 GHz were made on April 21, 1997, in a remote-observing mode from the Astro Space Center in Moscow. The 133 GHz observations are described in Slysh et al. (1997). The observing mode, receiver, and spectrometer setup for the 166 GHz observations were the same as for the 157 GHz observations.

The spectra were calibrated using the standard vane method (Kutner & Ulich, 1981). The accuracy of calibration is better than 10% (Kutner, personal communication).

The observed transitions are shown in Fig. 1. The frequencies and line strengths are presented in Table 1. All the data were reduced with the NRAO software package UNIPOPS.

EDITOR: PLACE TABLE 1 HERE.

EDITOR: PLACE FIGURE 1 HERE.

### 3. Observational results

Seventy-three sources were detected at 157 GHz. Narrow maser lines were observed in 4, while broad quasi-thermal lines in 72. Negative 157 GHz results are given in Table 3.

At 133 GHz, our results are the following: 33 quasi-thermal sources and 7 masers were found in the  $6_{-1} - 5_0E$  line, 13 quasi-thermal sources in the  $6_2 - 7_1A^-$  line, and 12 emission sources in the  $5_{-2} - 6_{-1}E$  line. Six quasi-thermal sources and no masers were observed at 165 GHz. In this paper, we present our results on quasi-thermal emission; the results on the 157 and 133 GHz masers were presented elsewhere (Slysh et al. 1995, 1997, respectively).

Gaussian parameters of the detected 157 GHz lines together with the positive and negative 133 GHz data are presented in Table 2. The 157 GHz lines  $J = 1-3$  are heavily blended. To obtain parameters of the lines, we made an assumption for the majority of the sources that the LSR velocity is equal to the LSR velocity of the  $4_0 - 4_{-1}E$  line. The center velocity and width of quasi-thermal lines for all the sources are very similar, suggesting that approximately the same regions were probed in all lines.

EDITOR: PLACE TABLE 2 HERE.

EDITOR: PLACE TABLE 3 HERE.

EDITOR: PLACE FIGURE 2 HERE.

EDITOR: PLACE FIGURE 3 HERE.

EDITOR: PLACE FIGURE 4 HERE.

EDITOR: PLACE FIGURE 5 HERE.

EDITOR: PLACE FIGURE 6 HERE.

EDITOR: PLACE FIGURE 7 HERE.

EDITOR: PLACE FIGURE 8 HERE.

Table 2 shows that the intensity of the broad ( $\Delta V \geq 5 \text{ km s}^{-1}$ )  $3_0 - 3_{-1}E$  lines is often lower than the value that is obtained by interpolation of the intensities of other 157 GHz lines. This can be understood if the lines are optically thick. If overlapping lines arise in a common region, then the shape of a spectral feature formed by them is not identical to the sum of their shapes. This results from the non-linearity of the radiation transfer equation. We calculated the optical thickness profile  $\tau(\nu)$  for a blend of lines at the frequencies of the  $J = 1$  to 3 157 GHz lines, having identical peak opacities  $\tau_0$ . Then we simulated the shape of the blend, i.e., for a frequency of each spectral channel the value  $T(\nu) = T_{ex}(1 - e^{-\tau(\nu)})$  was calculated. Here  $T_{ex}$  is an arbitrarily chosen "excitation temperature" of the lines. We obtained Gaussian fits for the lines, from which the model blend consists, with the UNIPOPS package in the same manner as we reduced the observational data. This procedure was repeated for different linewidths and  $\tau_0$ . We found that for optically thick lines the results of the Gaussian fitting depend on the linewidth. If the linewidth is less than about  $5 \text{ km sec}^{-1}$ , the intensities of the fitting Gaussians remain approximately equal. For larger linewidths, the overlapping becomes significant and a decrease of the  $J = 3$  Gaussian relative to the neighboring  $J = 1$  and  $J = 2$  Gaussians appears. The amplitudes of the latter two lines remained approximately correct, i.e., equal to  $T_{ex}(1 - e^{-\tau_0})$ . Thus, we believe that the decrease of the  $3_0 - 3_{-1}E$  line intensities obtained from the Gaussian analysis can be attributed to the overlapping of optically thick lines.

## 4. Excitation temperature

### 4.1. Analysis

The excitation temperature is an important parameter of the molecular energy level population distribution. For a transition from the upper level  $u$  to the lower level  $l$  at the

frequency  $\nu$  the excitation temperature is defined as

$$T_{\text{ex}} = -\frac{h\nu}{k \ln \left( \frac{g_u N_u}{g_l N_l} \right)} \quad (1)$$

$N$  is the population and  $g$  is statistical weight of the upper and lower levels. In thermodynamic equilibrium, the energy level population follows the Boltzmann distribution, and the excitation temperature of each transition is equal to the gas kinetic temperature. Deviation from the thermodynamic equilibrium is common in the interstellar medium, and the excitation temperature is usually different from the kinetic temperature. In the low density regions collisional transitions are less frequent than radiative transitions which depopulate energy levels. In simple molecules—diatomic or linear—this leads to a decrease of the upper level population relative to the lower level population, and to a decrease of the excitation temperature. In complex polyatomic molecules like methanol the energy levels are connected by allowed radiative transitions with several different levels, and the radiative transitions may cause deviation of the population distribution from the Boltzmann distribution in either direction: the upper level population may decrease relative to the lower level population which means a decrease of the excitation temperature, or the upper level population may increase relative to the lower level population, meaning an increase of the excitation temperature. Further rise of the relative population of the upper level over the ratio of the statistical weights leads to a population inversion, which is described as a negative excitation temperature.

In this study we will use results of the measurements of line intensities of several interconnected transitions of methanol in the Galactic molecular clouds to derive the excitation temperature of some interesting transitions. One can determine the population ratio of two levels of a given transition from the measured intensity ratio of two lines emitted from the upper and lower levels of this transition to some other levels. If several lines are emitted from a given level, any line can be chosen. This method is based on a fact that the intensity of an optically thin line is determined by the spontaneous emission rate from the upper to the lower level of the given transition and the population of the upper level. Note that for a small optical depth absorption is negligible and the line intensity does not depend on the population of the lower level.

The level population  $N$  is related to the intensity of a line, emitted from this level by the usual equation

$$\frac{N}{g} = \frac{3kW}{8\pi^3\nu S\mu^2} \quad (2)$$

where  $W = \int_v T_R dv$  is the integrated over the line profile radiation temperature,  $\mu$  and  $S$  are permanent dipole moment and line strength. Substituting the level populations from Eq. (2) into the equation for the excitation temperature (1) one obtains

$$T_{\text{ex}} = -\frac{h\nu}{k \ln\left(\frac{S_l\nu_l W_u}{S_u\nu_u W_l}\right)} \quad (3)$$

where  $S_u$ ,  $\nu_u$ ,  $W_u$  and  $S_l$ ,  $\nu_l$ ,  $W_l$  refer to the line strength, transition frequency and integrated radiation temperature of lines, emitted from the upper and lower level, respectively. Note, that Eq. (2) provides population of a given level even if the level gains or loses population via several transitions. Hence, Eq. (3) provides excitation temperature in multi-level systems, such as the methanol molecule. In this study excitation temperature of the  $6_{-1} - 5_0E$  transition was determined using the observed intensity of the same transition  $6_{-1} - 5_0E$  as a measure of the column density of the upper level  $6_{-1}E$ , and the intensity of the transition  $5_0 - 5_{-1}E$  as a measure of the column density of the lower level  $5_0E$ . Similarly, the excitation temperature of the transition  $5_0 - 4_0E$  was determined from the observed intensity ratio of the transitions  $5_0 - 5_{-1}E$  and  $4_0 - 4_{-1}E$ , giving the column density of the upper and lower levels, respectively. It is interesting that in this particular case the transition  $5_0 - 4_0E$  at 96 GHz was not observed in this study, and its excitation temperature has been derived from observations of two other transitions. The third transition, for which the excitation temperature was determined is  $5_{-2} - 6_{-1}E$ , for which the population ratio was found from the observed intensity ratio of the transitions  $5_{-2} - 6_{-1}E$  and  $6_{-1} - 5_0E$ . In some sources the line  $6_{-1} - 5_0E$  contains both narrow maser and broad quasi-thermal components. The results for the excitation temperature in this study refer to the quasi-thermal component. The excitation temperature for the transitions  $6_0 - 6_{-1}E$  and  $7_1 - 7_0E$  was determined from the intensity ratio of the pairs of lines  $(6_0 - 6_{-1}E)/(6_{-1} - 5_0E)$  and  $(7_1 - 7_0E)/(7_0 - 7_{-1}E)$ , respectively, which were observed in several sources.

From the observations, we obtain the beam-averaged brightness temperature rather than



the brightness temperature of the objects. The ratio of the upper-level populations, and hence, the excitation temperature may be affected by the different beam filling factors at 133, 157 and 165 GHz. We calculated the excitation temperatures for two extreme cases: (1) the sources uniformly fill the beams and (2) the sources are much smaller than the beams. In the former case, we can substitute the radiation temperature in Eq. (3) for the antenna temperature. In the latter case, introducing a beam filling factors leads to the expression

$$T_{\text{ex}} = - \frac{h\nu}{k \ln \left( \frac{S_l \nu_l^3 W_u}{S_u \nu_u^3 W_l} \right)} \quad (4)$$

which differs from (3) only by the exponent of the frequency ratio. Since this ratio is not far from unity (1.18 or 1.05), the difference between excitation temperatures determined by (3) and (4) is not significant, as can be seen in Table 5, except the case when the absolute value of the excitation temperature is large and its determination is critically dependent on parameters.

## 4.2. Results

We derived excitation temperature for the  $5_0 - 4_0E$ ,  $5_{-2} - 6_{-1}E$ ,  $6_{-1} - 5_0E$ , and  $7_1 - 7_0E$  transitions. The results are shown in Fig. 9 and Table 5<sup>1</sup>. The derived excitation temperature was found to be different for all transitions, meaning that the population distribution is not a Boltzmann distribution. The mean harmonic excitation temperature  $M(T_{\text{ex}})$  of the  $5_0 - 4_0E$  transition is 20 K (Fig. 9). This value is typical for the kinetic temperature in molecular clouds. Very strong deviations from this temperature are found in the other two transitions,  $6_{-1} - 5_0E$

---

<sup>1</sup>Microwave background cannot not be taken into account in this study and is neglected here. Using Eq. A3 from Turner (1991) we estimated that this can result in an overestimation of the excitation temperature of the subthermally excited Class II transitions, presented in Table 5. The overestimation may be of order of 1.5 if the excitation temperature, given in Table 5 is lower than 10 K. For the  $5_0 - 4_0E$  and  $6_{-1} - 5_0E$  transitions the errors, caused by this simplification are smaller and typically within the errors, presented in the table.

and  $5_{-2} - 6_{-1}E$ . The transition  $6_{-1} - 5_0E$  was found to be either inverted or overheated. The mean harmonic excitation temperature for our sample is  $M(T_{ex}) = -10$  K.

EDITOR: PLACE FIGURE 9 HERE.

The  $5_{-2} - 6_{-1}E$  transition demonstrates an opposite behaviour: it is overcooled in most sources, with the mean harmonic excitation temperature  $M(T_{ex}) = 5$  K, which is markedly less than the excitation temperature of the  $5_0 - 4_0E$  transition. The difference between excitation temperature of the three transitions is clearly visible from the comparison of the respective histograms (Fig. 9). The histograms were plotted for inverse excitation temperature  $1/T_{ex}$ , in order to avoid discontinuity in the transition from positive to negative temperature, which occurs through the infinity.

The  $6_0 - 6_{-1}E$  transition is also subthermally excited in most sources. It is inverted in W3(OH), provided that the source is extended. However, the source is most likely much smaller than our beam (see, e.g., Kalenskii et al. 1997); in this case the  $6_0 - 6_{-1}E$  transition is not inverted and its excitation temperature is lower than that of the  $5_0 - 4_0E$  transition.

The  $7_1 - 7_0E$  transition is inverted in W3(OH) and Cep A. In 345.01+1.79, it is subthermally excited.

## 5. Statistical equilibrium calculations.

In order to demonstrate how physical conditions in molecular clouds can cause the observed deviations from the equilibrium Boltzmann distribution we calculated several models in the Large Velocity Gradient (LVG) approximation, varying density and an external radiation intensity. Models a and b were calculated for warm gas with predominantly collisional excitation. Models c and d take into account external radiation. The modelling was performed using an LVG code, made available by C.M. Walmsley (Walmsley et al. 1988). The results are presented in Figure 10 and Table 6. The collisional selection rules are based on the paper by Lees & Haque (1974) and

imply that the  $\Delta K = 0$  collisions are preferred. These collisional selection rules are known to be not accurate enough, leading to attempts (not fully successful) to derive them from astronomical observations (Sobolev, 1990; Turner, 1998). The opacities determined by the LVG calculations, are small for all lines, presented in Table 6 in all models, except for the line  $5_0 - 4_0E$ , which has optical depth 1.1 in model d.

In the absence of external radiation, except for the microwave background (model a), the levels in the backbone ladder ( $K = -1$  for  $E$ -methanol) are overpopulated relative to those from adjacent ladders, and transitions with upper levels on the backbone ladders and lower levels on lateral ladders, like  $6_{-1} - 5_0E$  (Class I transitions), are inverted, whereas the transitions like  $5_{-2} - 6_{-1}E$  and  $J_0 - J_{-1}E$ , with upper levels on lateral ladders and lower levels on the backbone ladder (Class II transitions), are overcooled (The classification of methanol transitions is presented, e.g. in Menten (1991); Sobolev (1993); see also Table 1). The reason for the inversion of Class I transitions is a much longer lifetime against spontaneous decay of the upper level ( $6_{-1}E$ ), which belongs to the backbone ladder, as compared to the lower level ( $5_0E$ ). The inversion disappears if the density is  $10^7 \text{ cm}^{-3}$  (model b). External radiation alters the inversion. It populates more efficiently levels with shorter lifetimes against spontaneous decay, i.e., those on lateral ladders (Kalenskii 1995). If the radiation temperature exceeds the kinetic temperature, then the lateral ladders become more populated than the backbone ladder, leading to the inversion of some Class II transitions and disappearance of the inversion in Class I transitions (Cragg et al. 1992). For example, if the radiation temperature is 50 K, then in a cold (25 K) gas the Class II  $2_0 - 3_{-1}E$  transition is inverted (model c). However, this radiation is not strong enough to invert some other Class II lines, in particular, the  $J_0 - J_{-1}E$  or  $7_1 - 7_0E$  lines. Stronger radiation ( $T_{\text{RAD}} = 150 \text{ K}$ , model d) can invert these lines, too.

EDITOR: PLACE TABLE 6 HERE.

The  $5_0 - 4_0E$  line remains thermally excited with or without external radiation, with the excitation temperature slowly growing with the radiation temperature and close to the gas kinetic

temperature, unless the density is lower than  $10^5 \text{ cm}^{-3}$  (model a). This can be the case for sources with a strongly inverted  $6_{-1} - 5_0E$  line, i.e., when the absolute value of the  $6_{-1} - 5_0E$  transition excitation temperature is about 10 K or lower.

EDITOR: PLACE FIGURE 10 HERE.

## 6. Discussion

The observations show that in the majority of sources the  $6_{-1} - 5_0E$  transition is inverted, while the  $5_{-2} - 6_{-1}E$  transition is overcooled. This agrees with the models a and b, meaning that the collisional excitation alone can lead to the inversion or overcooling of some methanol transitions.

EDITOR: PLACE TABLE 5 HERE.

The excitation temperature of the Class I  $6_{-1} - 5_0E$  transition is negative in the majority of sources, i.e. the lines are inverted. The  $1/ \langle T_{\text{ex}} \rangle$  value is equal to  $-0.1$ . SE calculations show that the  $6_{-1} - 5_0E$  transition is inverted if the density is lower than  $10^7 \text{ cm}^{-3}$ , and external radiation is absent or weak. Thus, we can conclude that in most observed sources the gas density is below  $10^7 \text{ cm}^{-3}$ , and there is no significant external radiation.

In spite of the inversion of the  $6_{-1} - 5_0E$  transition, the sources show thermal emission profiles, without line narrowing, typical for maser emission. This is possible for low optical depth when the maser gain is less than unity and the line narrowing does not occur. According to Sobolev (1993), such objects can be called Class Ib masers.

In contrast to this, the excitation temperature of the Class II  $5_{-2} - 6_{-1}E$  and  $6_0 - 6_{-1}E$  transitions is typically positive and much lower than the excitation temperature of the  $5_0 - 4_0E$  transition. Since the  $5_0 - 4_0E$  transition is thermally or subthermally excited, the excitation of

the  $5_{-2} - 6_{-1}E$  and  $6_0 - 6_{-1}E$  transitions is typically subthermal. The reason for the subthermal excitation of these Class II lines is the same as for the inversion of the  $6_{-1} - 5_0E$  transitions, i.e. much longer lifetime against spontaneous decay of the levels on the backbone ladder. In the case of the  $5_{-2} - 6_{-1}E$  and  $6_0 - 6_{-1}E$  transitions, the lower level,  $6_{-1}E$ , belongs to the backbone ladder and is overpopulated relative to the upper  $5_{-2}E$  or  $6_0E$  levels.

SE calculations indicate that the inversion of the transitions that belong to Class II requires a strong radiation field (see also Cragg et al. (1992); Sobolev et al. (1997)). Since strong radiation is necessary to invert the  $7_1 - 7_0E$  transition (Table 5; Sobolev et al. 1997), it may belong to Class II. The  $7_1 - 7_0E$  transition proved to be inverted in W3(OH) and Cep A. According to current models of methanol excitation, the inversion of Class I transitions prohibits the inversion of Class II transition in the same region, and vice versa. Hence, the transitions  $6_{-1} - 5_0E$  and  $7_1 - 7_0E$ , which belong to Class I and II, respectively, cannot be inverted simultaneously. For W3(OH) and Cep A, both of these transitions appear inverted, in conflict with this statement. Most likely, the inversion of either or both of these transitions is spurious and caused by a combination of calibration/optical depth effects (see the next section). However, a complex source structure is possible or the  $7_1 - 7_0E$  transition may not belong to Class II.

For the  $5_0 - 4_0E$  transition, we obtained positive excitation temperatures. The  $1/ \langle T_{\text{ex}} \rangle$  value is equal to 0.05. It is known from SE calculations that the  $5_0 - 4_0E$  transition is not inverted over the whole range of temperature, density, and methanol abundance typical for Galactic molecular clouds, and its excitation temperature is close to the kinetic temperature, unless the gas density is about  $10^5 \text{ cm}^{-3}$  or lower. In the latter case, the excitation temperature of the  $5_0 - 4_0E$  transition is lower than the kinetic temperature. According to Table 5, such low density implies a strong inversion of the  $6_{-1} - 5_0E$  transition. Hence, in the sources with a strongly inverted  $6_{-1} - 5_0E$  transition, i.e., those with the absolute value of the  $6_{-1} - 5_0E$  transition excitation temperature about 10 K or lower, (see Table 6), the  $5_0 - 4_0E$  transition may be subthermally excited, whereas for all other sources the excitation temperature of the  $5_0 - 4_0E$  line  $T_{54}$  represents the kinetic temperature. Table 5 shows that in the majority of the observed objects,  $T_{54}$  is limited

to 15–50 K. Therefore the kinetic temperatures of at least dense sources from our sample must be enclosed in the same range.

### 6.1. Optical depth effects

To estimate source properties, we made the usual assumption that the observed lines are optically thin. However, this assumption may not always be valid (see Kalenskii et al. 1997). A question arises whether the inversion, found in two lines, can be an artifact, caused by optical depth effects. If the excitation temperature is derived, as we do, from the ratio of the upper and lower level population, the transition can appear to be (but not actually be) inverted if the upper level population is overestimated, the lower level population is underestimated, or both. The population of the upper level will be overestimated if the line, used for derivation of the level’s column density, is optically thick and inverted. The population of the lower level will be underestimated if the line, observed for the derivation of the level’s column density, is optically thick and not inverted. We obtained inversion in the transitions  $6_{-1} - 5_0E$  and  $7_1 - 7_0E$ . The same transitions were used to determine their upper level populations (see Table 4). Therefore optical depth can lead to overestimation of the upper level population only if these transitions are really inverted. Hence, these transitions can appear as inverted, being not inverted, only if the transitions used to determine the lower level population ( $5_0 - 5_{-1}E$  and  $7_0 - 7_{-1}E$ , respectively) are not inverted and are optically thick, leading to underestimation of the  $5_0E$  and  $7_0E$  level population.

EDITOR: PLACE TABLE 7 HERE.

Below, we discuss whether optical depth can lead to apparent detection of inversion in the  $6_{-1} - 5_0E$  transition. We could not estimate the optical depth effect quantitatively, since the optical depth of the observed  $6_{-1} - 5_0E$  and  $5_0 - 5_{-1}E$  lines (see Table 4) is unknown. We can not find excitation temperature, corrected for optical depth effect. Instead, we estimated how large

the optical depth of the  $5_0 - 5_{-1}E$  line must be in order to cause the apparent inversion of the  $6_{-1} - 5_0E$  transition. We assume that the  $6_{-1} - 5_0E$  line is optically thin; this is the best case for the appearance of a spurious inversion, since in the opposite case the ratio of the  $6_{-1}E$  and  $5_0E$  level population becomes lower, decreasing the chance for the spurious inversion to appear. We corrected the population of the  $5_0E$  level for the optical depth effect

$$\frac{N'_u}{g'_u} = \frac{N_u}{g_u} \frac{\tau}{1 - \exp(-\tau)} \quad (5)$$

where  $N_u/g_u$  is the value obtained in the optically thin approximation, assuming optical depth of the  $5_0 - 5_{-1}E$  line of 1, 2, and 3. Higher optical depth is not likely, according to Kalenskii et al. (1997). Then, using these corrected values, we calculated the  $6_{-1} - 5_0E$  transition excitation temperature. The same procedure was applied for the  $7_1 - 7_0E$  transition, i.e., we assumed that the  $7_1 - 7_0E$  line is optically thin and examined how large optical depth of the  $7_0 - 7_{-1}E$  line should be to cause the apparent inversion of the  $7_0 - 7_{-1}E$  transition. The results are shown in Table 7, and can be summarized for the  $6_{-1} - 5_0E$  transition as follows:

- an optical depth equal to 1, "quenches" the inversion if the modulus of the initial excitation temperature (i.e., that presented in Table 5) is of the order of or larger than 10 K.
- if the modulus of the initial excitation temperature is of the order of or less than 5, then the inversion does not disappear, even if the optical depth is equal to 3.

Thus, in most of the sources, given in Table 5, the derived inversion of the  $6_{-1} - 5_0E$  transition cannot be an artifact caused by optical depth effects.

For the  $7_1 - 7_0E$  transition, inversion was found in W3(OH) and Cep A. Table 7 shows that optical depth of the  $7_0 - 7_{-1}E$  transition of order 1 or larger can cause apparent detection of this inversion.

The excitation temperature of the thermal  $5_0 - 4_0E$  transition was calculated from the ratio of the  $5_0 - 5_{-1}E$  and  $4_0 - 4_{-1}E$  line intensities. With the increase of optical depth, this ratio tends to unity, and the excitation temperature calculated from Eq. 1 tends to 69 K, independent

of the real excitation temperature. However, we calculated a number of models and found that optical depths of the  $4_0 - 4_{-1}E$  line as high as 3 can lead to  $T_{54}$  errors not larger than 1.5. Hence, the excitation temperature of the  $5_0 - 4_0E$  transition given in Table 5 is not affected seriously by optical depth effects.

## 7. Summary and conclusions

1. We observed a large sample of star-forming regions in the  $J_0 - J_{-1}E$  series of methanol lines near 157 GHz. Emission was detected toward 73 sources. Many of them were additionally observed in the  $6_{-1} - 5_0E$ ,  $6_2 - 7_1A^-$ , and  $5_{-2} - 6_{-1}E$  lines near 133 GHz and six sources were observed in the  $7_1 - 7_0E$  line at 166 GHz. The observations at 133 and 166 GHz were made in a remote observing mode from the Astro Space Center in Moscow.
2. The excitation of methanol transitions proved to be quite diverse. Typically, the  $6_{-1} - 5_0E$  transition is inverted, showing that in most observed sources the gas density is below  $10^7 \text{ cm}^{-3}$  and there is no significant external radiation. The  $5_{-2} - 6_{-1}E$  and  $6_0 - 6_{-1}E$  transitions are overcooled and the  $5_0 - 4_0E$  transition is thermally excited. The  $7_1 - 7_0E$  transition may be inverted in W3(OH) and Cep A, indicating that a strong radiation field in these sources may be present.

We are grateful to Dr. Phil Jewell and the staff of the Kitt-Peak 12-m telescope for help during the observations. We would like to thank Dr. Garwood (NRAO) for providing the UNIPOPS package. The work was done under partial financial support from the Russian Foundation for Basic Research (grant No 95-02-05826), International Science Foundation (grants No MND000 and MND300), and European Southern Observatory. The Sun Sparc station used in the remote observations was made available to the Astro Space Center through a grant from the National Science Foundation to the Haystack Observatory.



## REFERENCES

- Ball, J. A., Gottlieb, C. A., Lilley, A. E., & Radford, H. E. 1970, *ApJ*, 162, L203.
- Cragg, D. M., Johns, K. P., Godfrey, P. D., & Brown, R.D. 1992, *MNRAS*, 259, 203.
- Kalenskii, S. V. 1995, *Astronomy Reports*, 39, 465.
- Kalenskii, S. V., Dzura, A. M., Winnberg, A., Booth, R., & Alakoz, A. 1997, *A&A*, 321, 311.
- Kutner, M. L., & Ulich, B. L. 1981, *ApJ*, 250, 341.
- Lees, R. M., Lovas, F. J., Kirchoff, W. H., & Johnson, D. R. 1973, *J. Phys. Chem. Ref. Data*, 2, 205.
- Menten, K. M., 1991. In: Haschick, A. D., Ho, P. T. P. (eds.) *Proc. of the Third Haystack Observatory Meeting, MA, USA, Skylines*. p. 119
- Menten, K. M., Walmsley, C. M., Henkel, C., & Wilson, T. L., 1988, *A&A*, 198, 253.
- Slysh, V. I., Kalenskii, S. V., & Val'tts, I. E. 1995, *ApJ*, 442, 668.
- Slysh, V. I., Kalenskii, S. V., Val'tts, I. E., & Golubev V.V. 1997, *ApJ*, 478, L37.
- Sobolev, A. M., 1990, *Kinematika i Fizika Nebesnykh Tel*, 6, 3.
- Sobolev, A. M., 1993, *Lecture Notes in Physics*, 412, 215.
- Sobolev, A. M., Cragg, D. M., & Godfrey, P. D., 1997, *MNRAS*, 288, L39-L43.
- Turner, B.E., 1998, *ApJ*, 501, 731.
- Walmsley, C. M., Batrla, W., Matthews, H. E., & Menten, K. M. 1988, *A&A*, 197, 271.
- Ziurys, L. M., & McGonagle, D., 1993, *ApJS*, 89, 155.

Fig. 1.— The energy level diagram of  $A$  and  $E$  methanol. The observed transitions are marked by arrows.

Fig. 2.— Spectra of the sources observed at 157 GHz. X-axis, LSR velocity of the  $1_0 - 1_{-1}E$  line; Y axis,  $T_R^*$ . Vertical bars in the upper spectra indicate the lines (from left to right):  $2_0 - 2_{-1}E$ ,  $3_0 - 3_{-1}E$ ,  $1_0 - 1_{-1}E$ ,  $4_0 - 4_{-1}E$ ,  $5_0 - 5_{-1}E$ .

Fig. 3.— Same as Fig.2

Fig. 4.— Same as Fig.2

Fig. 5.— Spectra of the sources observed at 133 GHz. Upper spectra,  $6_{-1} - 5_0E$  lines; middle,  $6_2 - 7_1A^-$  lines; lower,  $5_{-2} - 6_{-1}E$  lines.

Fig. 6.— Same as Fig. 5

Fig. 7.— Same as Fig. 5

Fig. 8.— Spectra of the sources observed at 166 GHz

Fig. 9.— The distribution of  $1/T_{\text{ex}}$  for various transitions.

Fig. 10.— Relative population of methanol- $E$  levels. Y-axis,  $\lg E$ -methanol level population relative to that of the ground level; X-axis, level energy in Kelvins. Solid line: levels belong to the backbone ladder,  $K = -1$ ; dashed line:  $K = 0$ ; dotted line:  $K = -2$ . The a, c, and d models are same as in Table 6.

Table 1. Frequencies and line strengths of the transitions observed at 133, 157, and 165 GHz  
(from Lees et al. 1973)

N	Transition	Frequency, MHz	Line Strength	Class
1	$1_0 - 1_{-1}E$	157270.70	0.7057	II
2	$2_0 - 2_{-1}E$	157276.04	1.1762	II
3	$3_0 - 3_{-1}E$	157274.47	1.6467	II
4	$4_0 - 4_{-1}E$	157246.10	2.1172	II
5	$5_0 - 5_{-1}E$	157178.97	2.5877	II
6	$6_0 - 6_{-1}E$	157048.62	3.0582	II
7	$7_0 - 7_{-1}E$	156828.52	3.5287	II
8	$8_0 - 8_{-1}E$	156488.95	3.9992	II
9	$6_{-1} - 5_0E$	132890.79	1.6467	I
10	$6_2 - 7_1A^-$	132621.94	0.9389	II
11	$5_{-2} - 6_{-1}E$	133605.50	0.8009	II
12	$7_1 - 7_0E$	166169.21	3.2412	II?

Table 3. Negative results at 157 GHz

Source	RA (1950)	DEC (1950)	LSR velocity km s <sup>-1</sup>	rms
173.59+02.24	05 36 06.4	35 29 21	-13.5	0.10
S255	06 10 01.0	18 00 44	4.5	0.11
352.51-0.15	17 23 48.5	-35 17 13	-52.0	0.02
10.33-0.17	18 06 06.7	-20 05 34	10.0	0.09
10.96+0.01	18 06 44.2	-19 27 35	24.0	0.08
12.03-0.04	18 09 07.4	-18 32 39	108.5	0.07
11.51-1.50	18 13 28.3	-19 42 25	7.0	0.06
20.24+0.08	18 24 55.8	-11 16 24	72.5	0.08
21.88+0.02	18 28 16.1	-09 51 01	21.5	0.05
22.35+0.05	18 29 01.0	-09 25 15	80.0	0.06
25.83-0.20	18 36 26.4	-06 27 14	92	0.10
W43M	18 45 36.8	-01 29 12	109.0	0.11
37.43+1.50	18 51 48.7	04 37 19	41.0	0.13
40.42+0.70	19 00 14.4	06 54 28	15.0	0.13
59.84+0.66	19 38 55.9	23 57 50	38.0	0.09
21007+4951	21 00 44.9	49 51 13	-1.0	0.12
R146	21 42 40.0	65 52 57	-6.4	0.07

Table 4. Line ratios used to derive the excitation temperature of methanol transitions

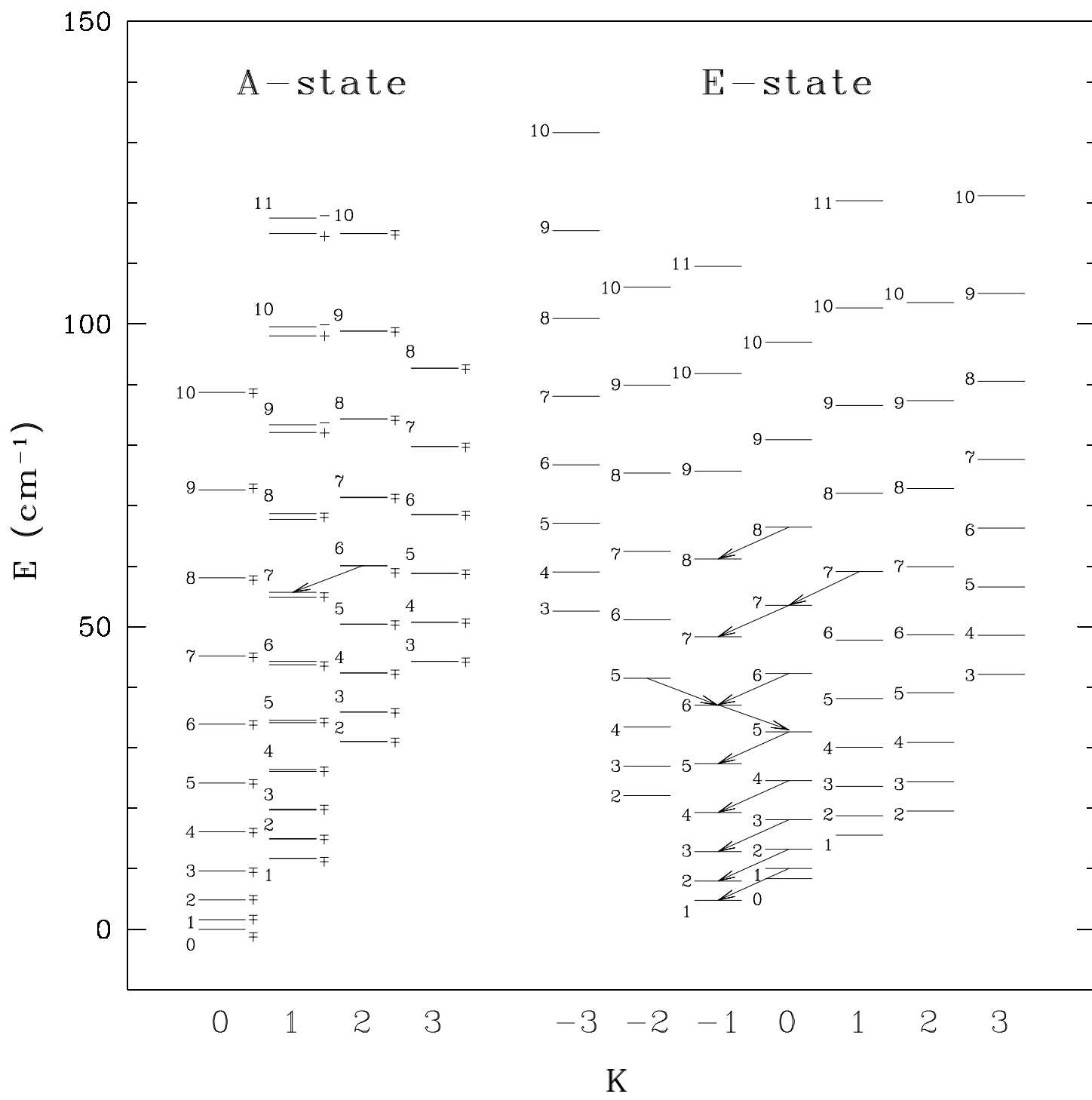
Transition	Line ratio
$6_{-1} - 5_0E$	$6_{-1} - 5_0E/5_0 - 5_{-1}E$
$5_{-2} - 6_{-1}E$	$5_{-2} - 6_{-1}E/6_{-1} - 5_0E$
$5_0 - 4_0E$	$5_0 - 5_{-1}E/4_0 - 4_{-1}E$
$6_0 - 6_{-1}E$	$6_0 - 6_{-1}E/6_{-1} - 5_0E$
$7_1 - 7_0E$	$7_1 - 7_0E/7_0 - 7_{-1}E$

Table 6. Excitation temperature of  $E$ -methanol transitions obtained from statistical equilibrium calculations. For all models  $T_{kin} = 25$  K. Other parameters are the following: model a:  $n_{H_2} = 1.0 \times 10^5$  cm,  $n_{CH_3OH-E}/(dV/dR) = 1.0 \times 10^{-4}$  cm $^{-3}/(\text{km s}^{-1}/\text{pc})$ ,  $T_{rad} = 2.7$  K. model b:  $n_{H_2} = 1.0 \times 10^7$  cm,  $n_{CH_3OH-E}/(dV/dR) = 1.0 \times 10^{-4}$  cm $^{-3}/(\text{km s}^{-1}/\text{pc})$ ,  $T_{rad} = 2.7$  K. model c:  $n_{H_2} = 1.0 \times 10^7$  cm,  $n_{CH_3OH-E}/(dV/dR) = 1.0 \times 10^{-4}$  cm $^{-3}/(\text{km s}^{-1}/\text{pc})$ ,  $T_{rad} = 50$  K. model d:  $n_{H_2} = 1 \times 10^7$  cm,  $n_{CH_3OH-E}/(dV/dR) = 1.0 \times 10^{-3}$  cm $^{-3}/(\text{km s}^{-1}/\text{pc})$ ,  $T_{rad} = 150$  K.

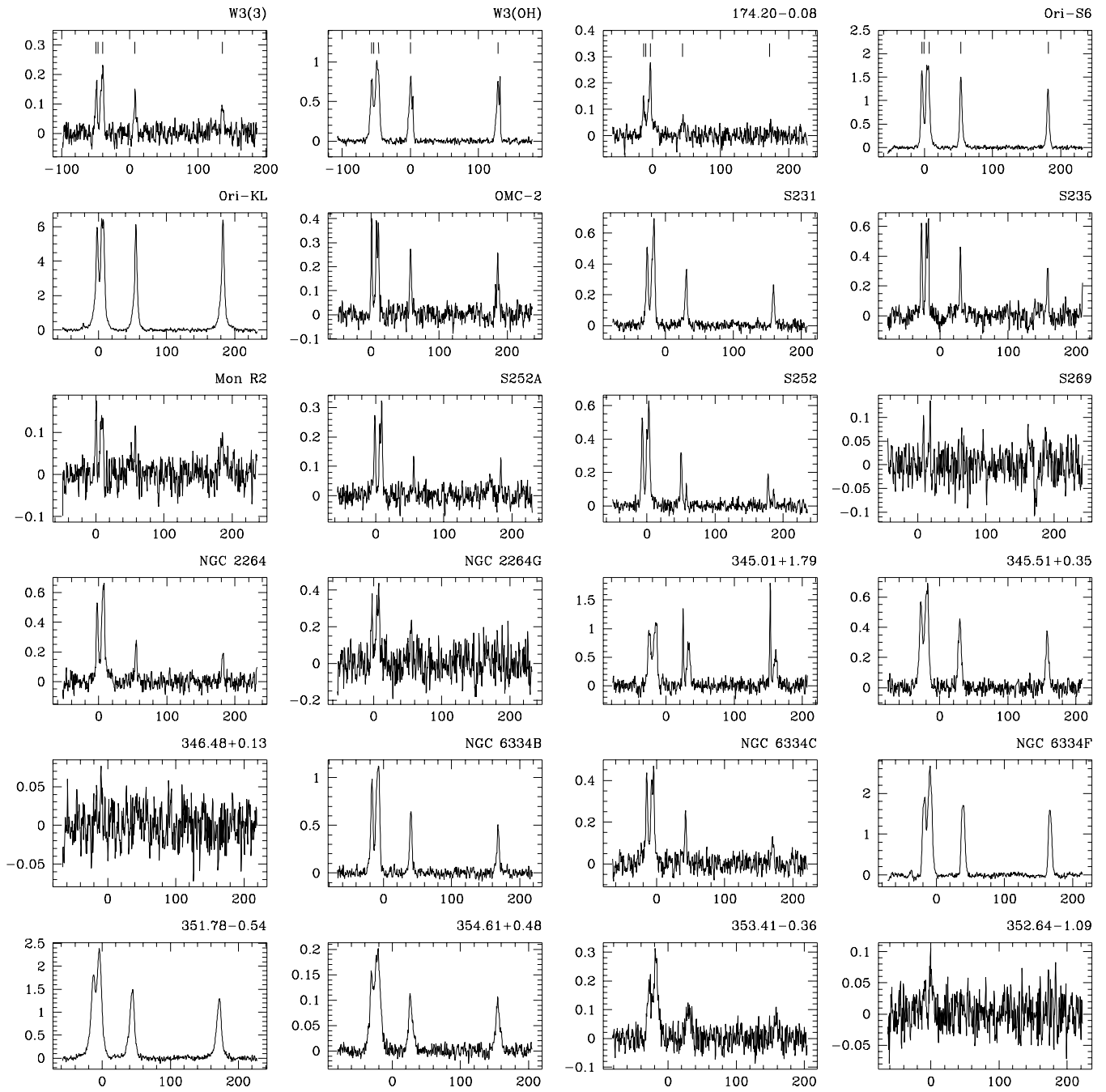
Transition	Model a	NGC6334F	Model b	Model c	W3(OH)	Model d
$5_{-2} - 6_{-1}E$	1.4	11.2	4.5	-28.8	13.4	-13.5
$6_{-1} - 5_0E$	-4.9	-40	106.9	16.5	29	12.9
$4_0 - 4_{-1}E$	3.3		15.1	50.6		-145.0
$5_0 - 4_0E$	11.1	38	24.2	25.6	24	27.5
$7_1 - 7_0E$	2.9		12.5	75.0	-8	-74.0
$2_0 - 3_{-1}E$	0.4		2.8	-4.6		-1.7

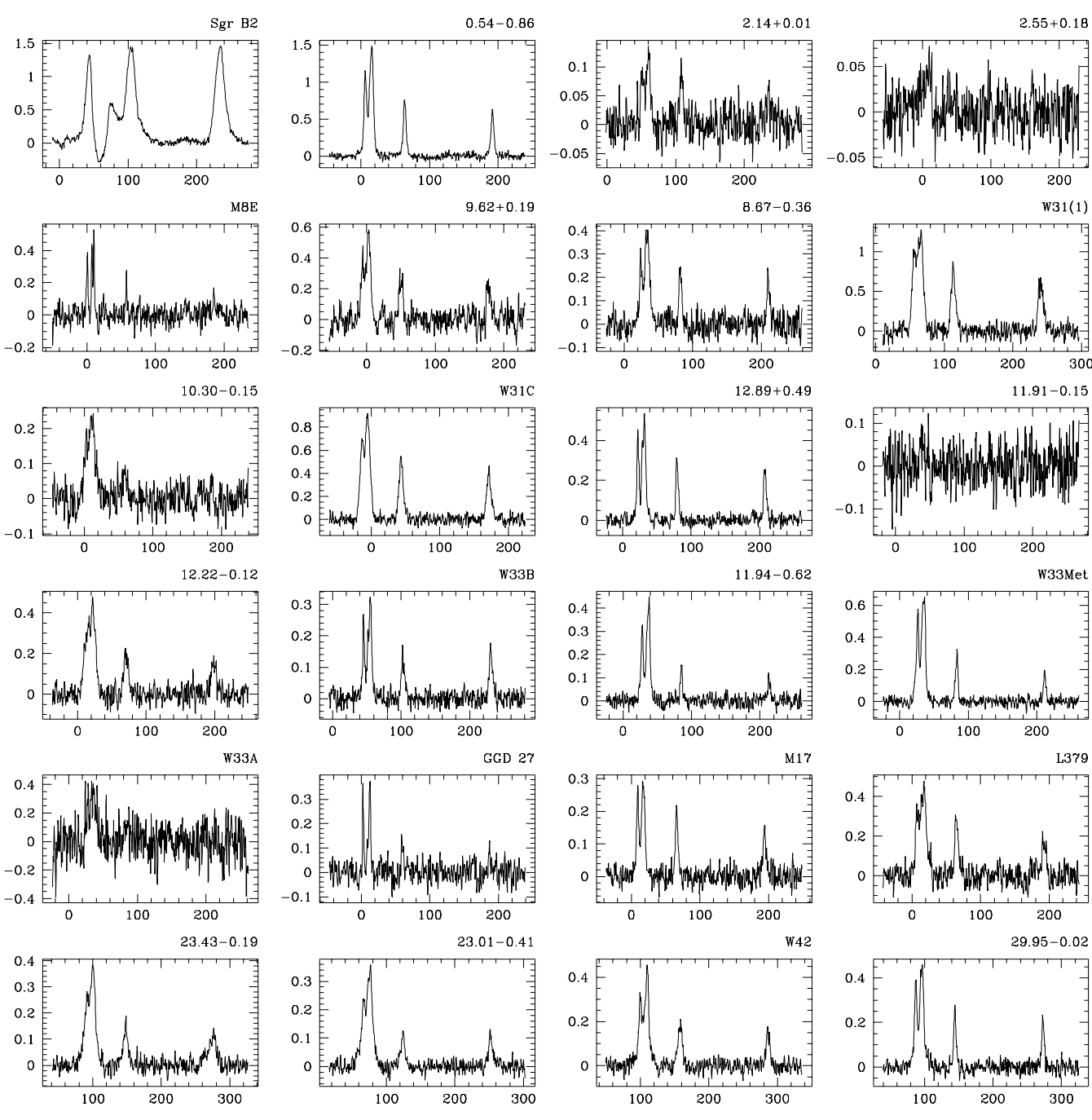
Table 7. Excitation temperature of the  $6_{-1} - 5_0E$  and  $7_1 - 7_0E$  transitions, corrected for optical depths of the  $5_0 - 5_{-1}E$  and  $7_0 - 7_{-1}E$  lines, respectively

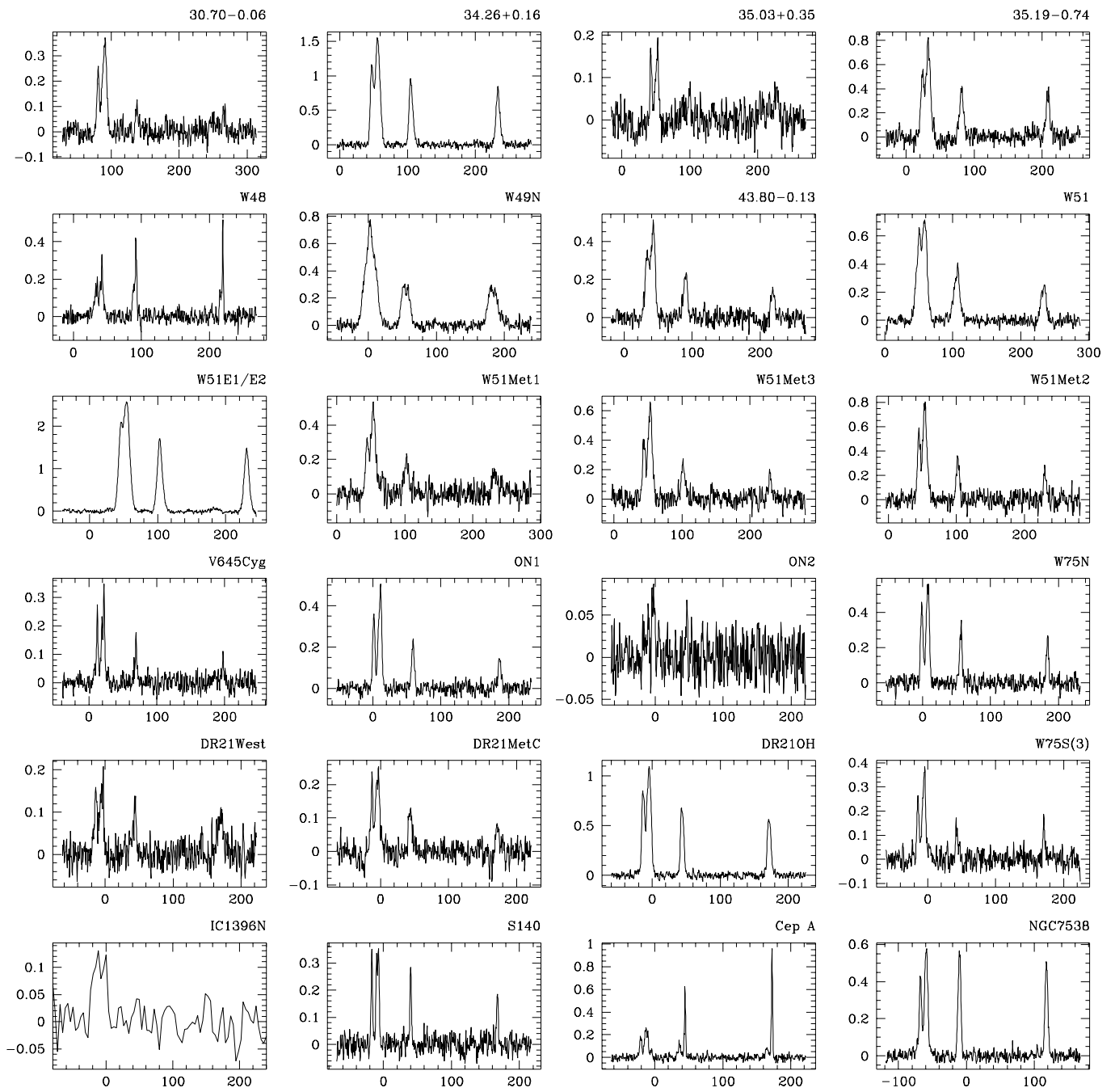
$T_{ex}$	$6_{-1} - 5_0E$			$7_1 - 7_0E$			
	opt. thin	$\tau = 1$	$\tau = 2$	$\tau = 3$	$\tau = 1$	$\tau = 2$	$\tau = 3$
-3		-3.8	-4.9	-6.5	-3.6	-4.4	-5.2
-5		-7.8	-14.6	-50.5	-7.0	-10.6	-17.9
-7						-26.6	717
-10		-35.6	31.8	12.5	-23.6	191.8	22.6
-15			15.4	8.8	-109.7	25.9	12.9

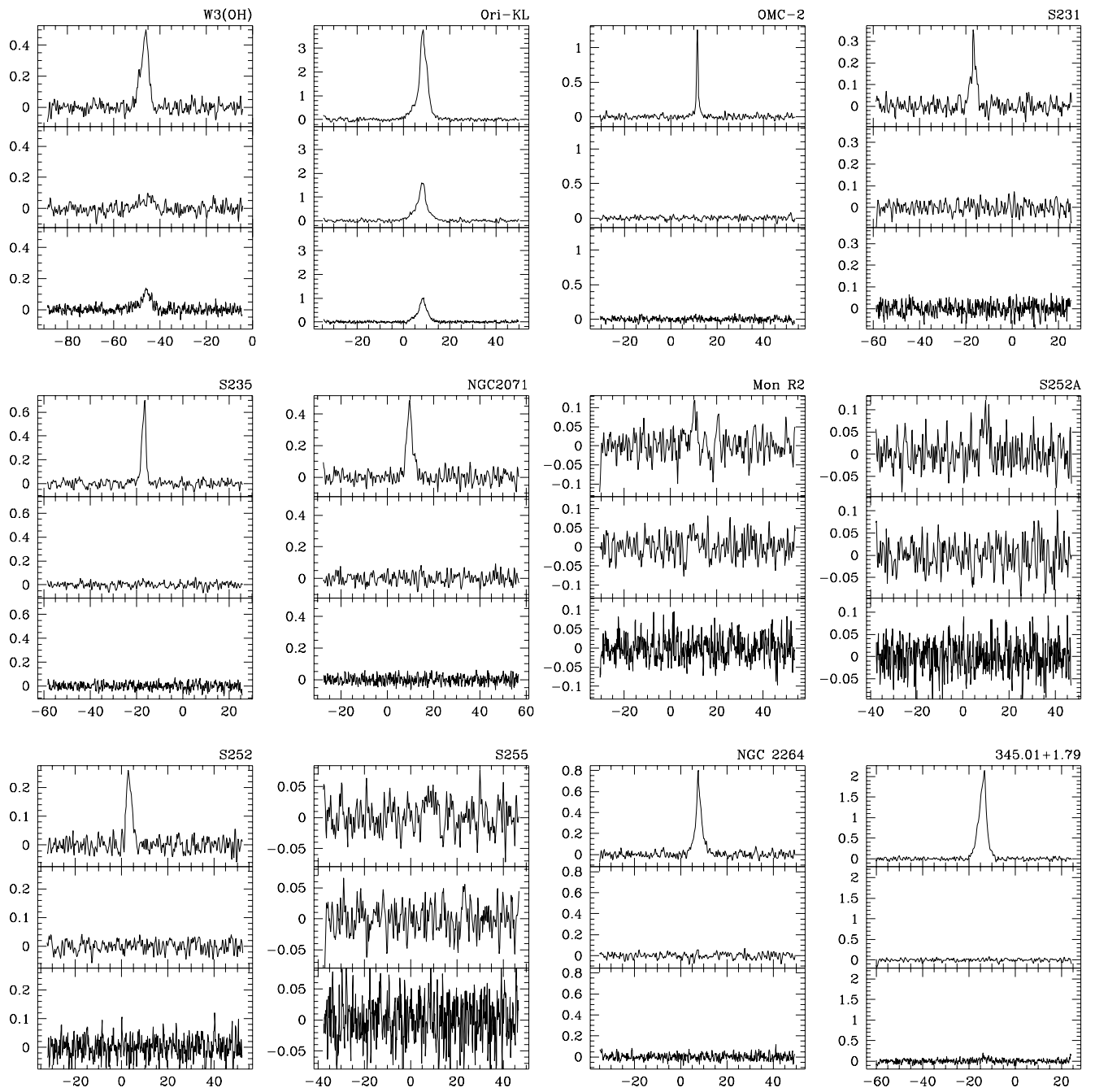


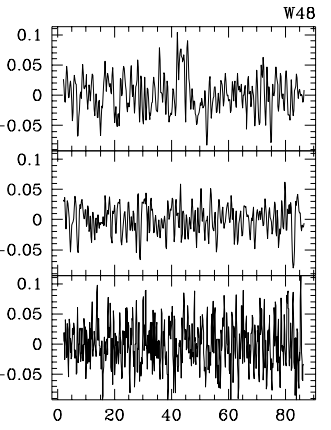
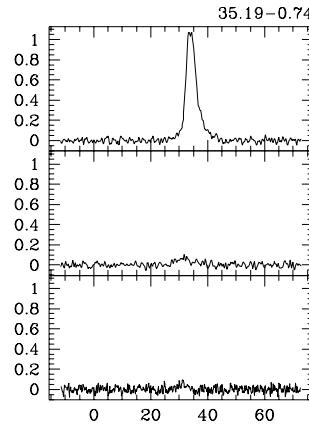
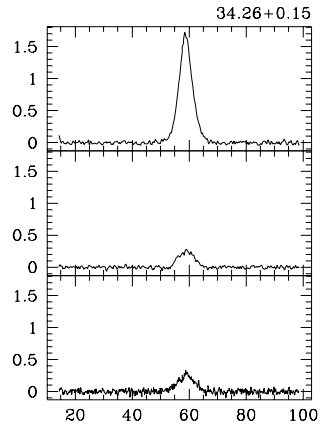
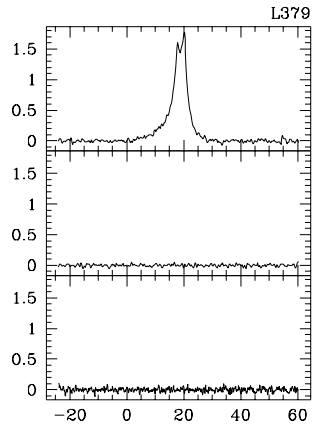
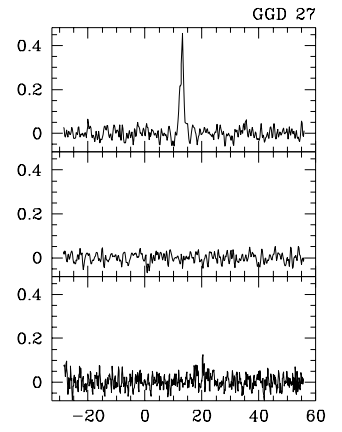
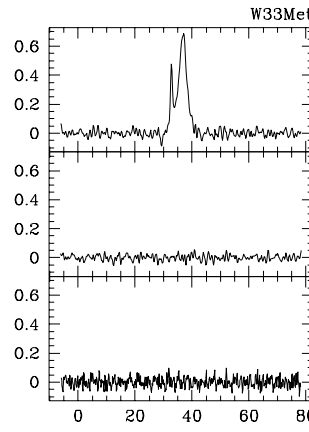
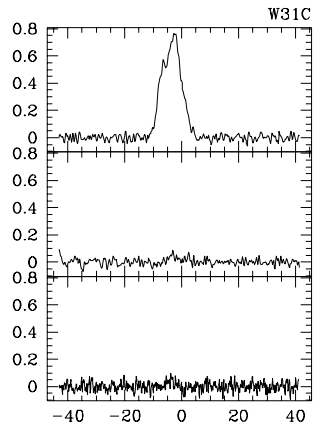
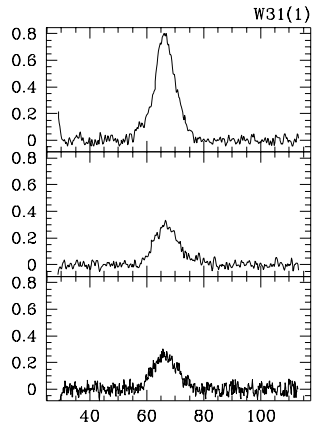
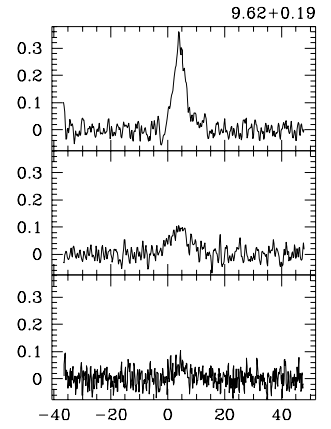
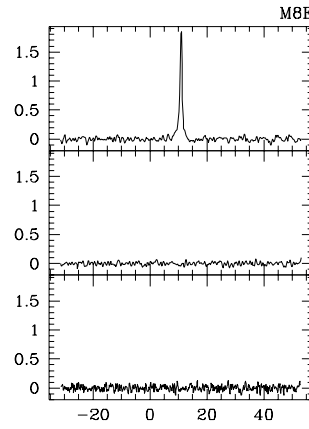
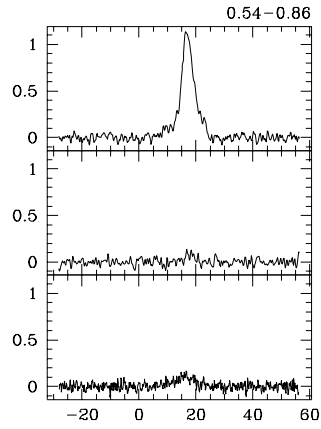
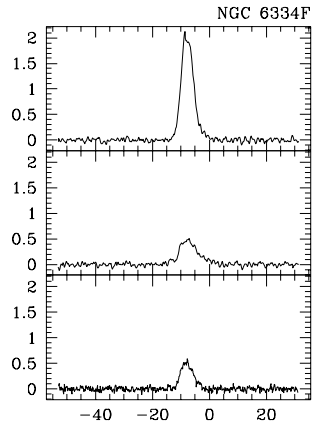


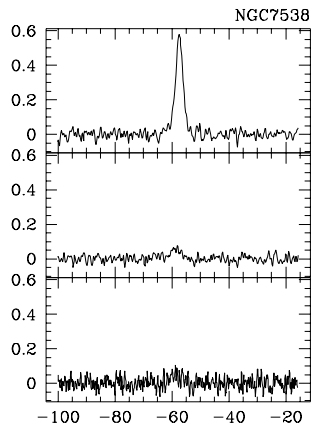
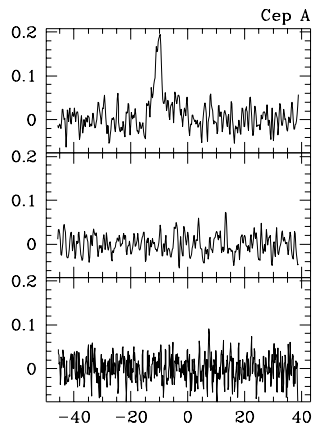
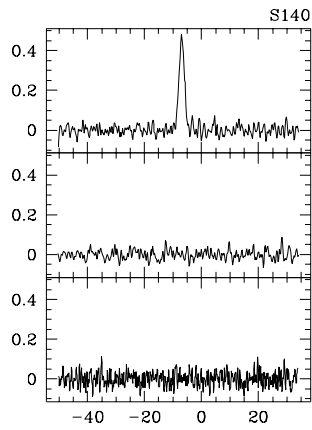
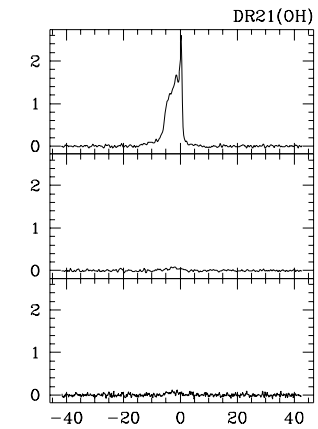
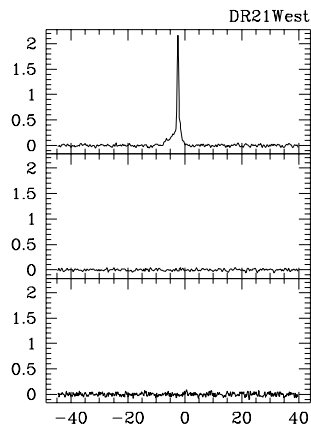
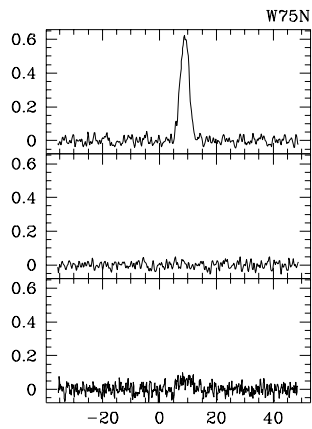
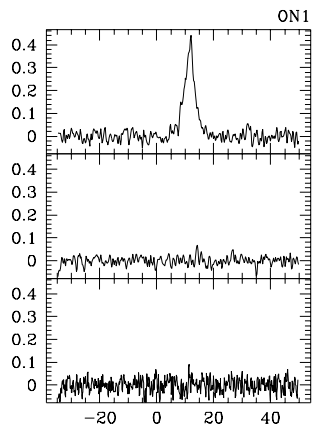
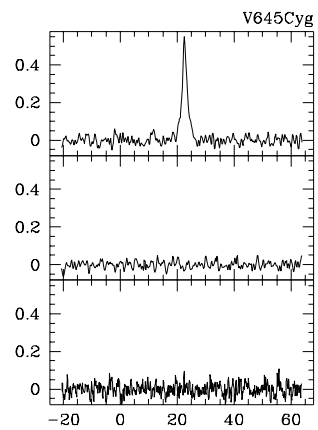
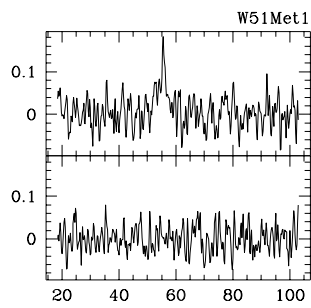
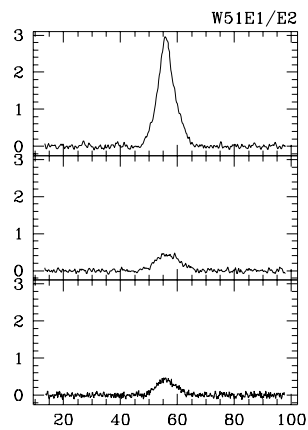
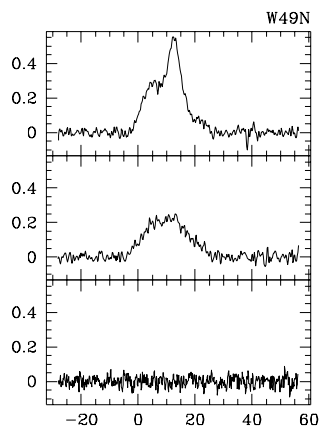


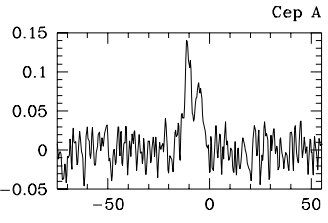
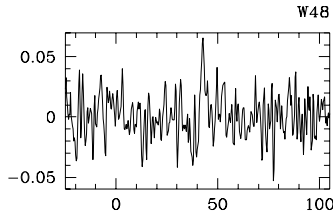
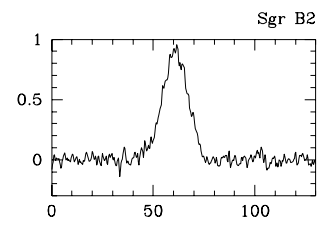
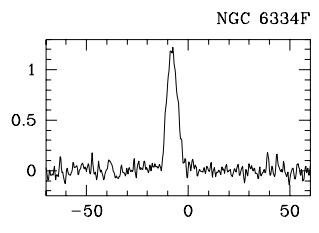
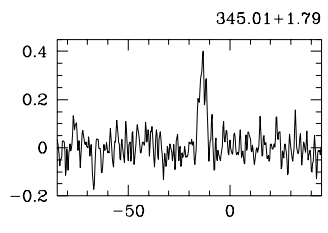
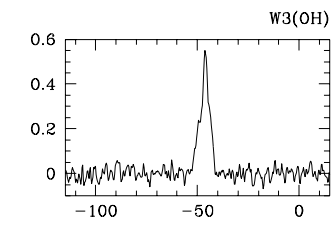


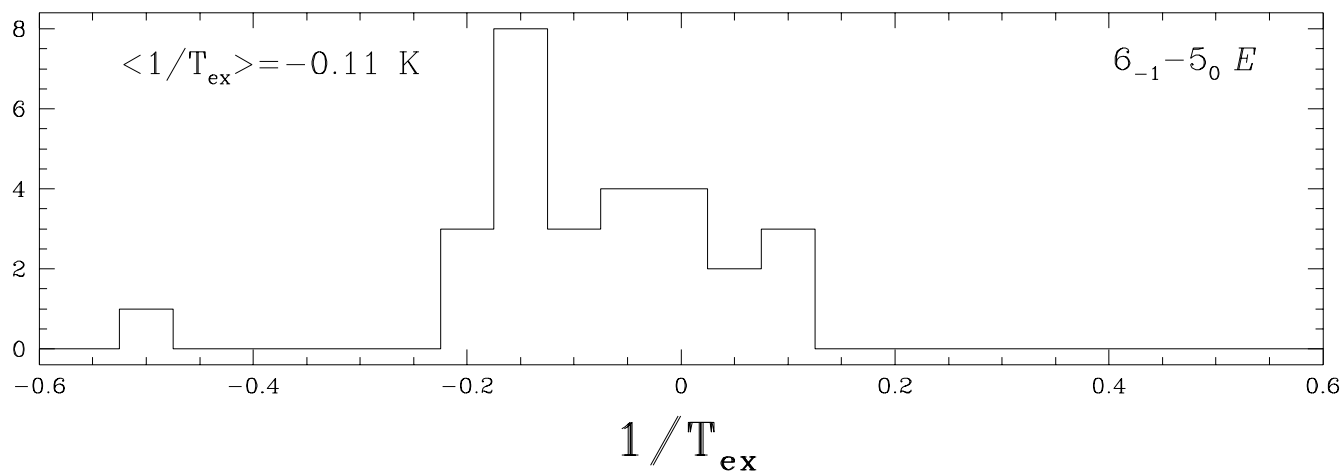
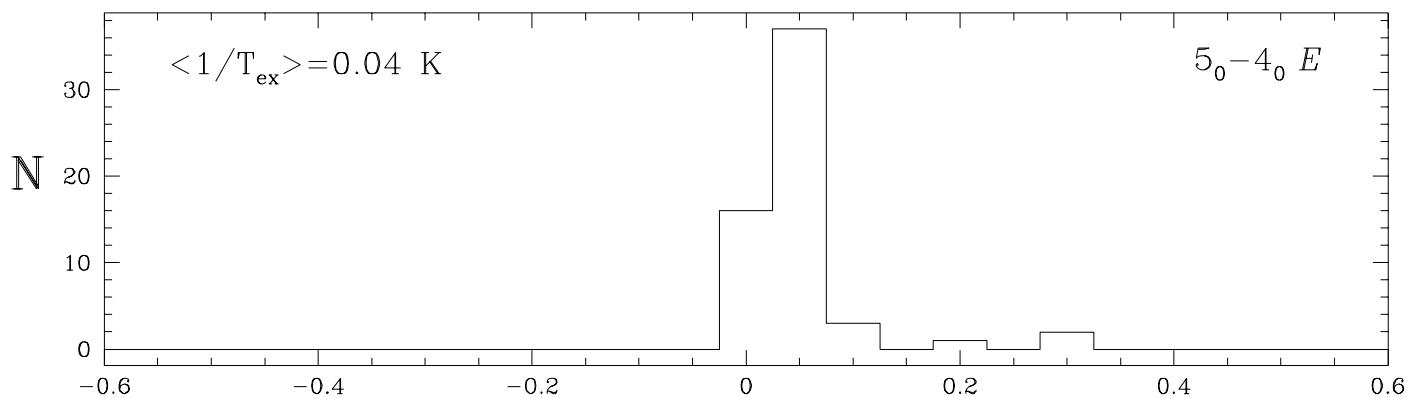
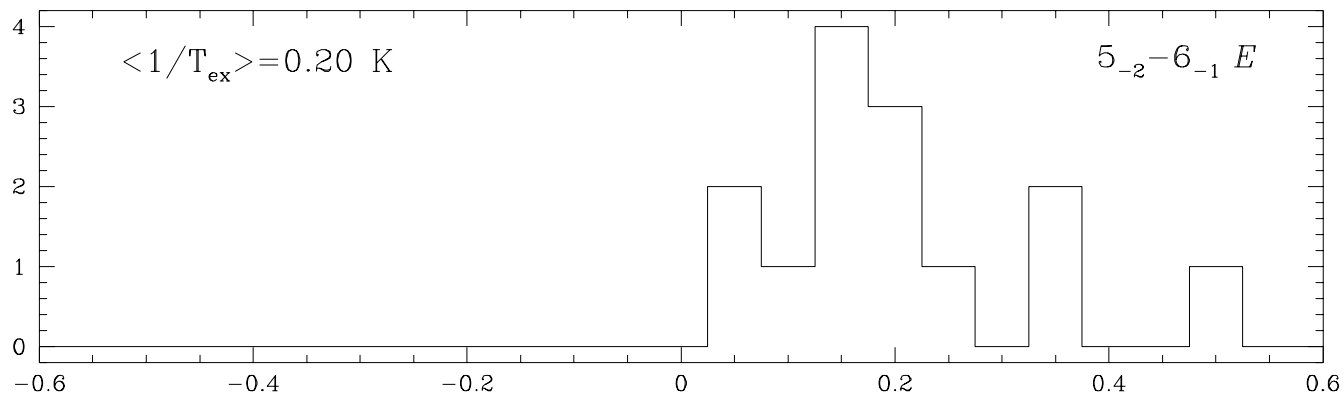














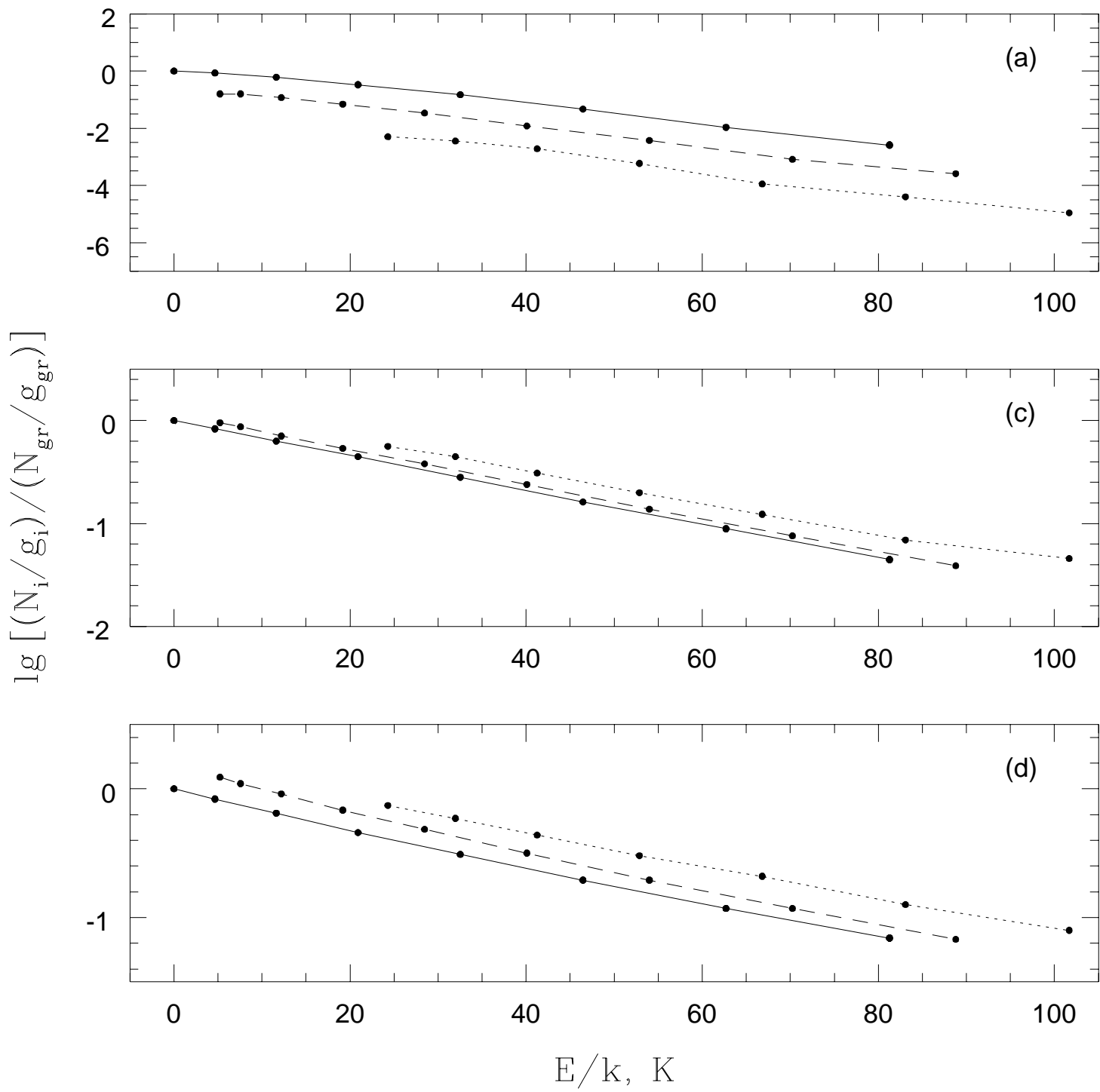


TABLE 2

RESULTS OF THE OBSERVATIONS AT 133, 157, AND 165 GHz. THE NUMBERS IN COLUMN 4 CORRESPOND TO THE LINES: 1,  $1_0 - 1_{-1}E$ ; 2,  $2_0 - 2_{-1}E$ ; 3,  $3_0 - 3_{-1}E$ ; 4,  $4_0 - 4_{-1}E$ ; 5,  $5_0 - 5_{-1}E$ ; 6,  $6_0 - 6_{-1}E$ ; 7,  $7_0 - 7_{-1}E$ ; 8,  $8_0 - 8_{-1}E$ ; 9,  $5_{-2} - 6_{-1}E$ ; 10,  $6_2 - 7_1A^-$ ; 11,  $6_{-1} - 5_0E$ ; 12,  $7_1 - 7_0E$ . THE UPPER LIMITS FOR NON-DETECTIONS ARE GIVEN AT THE  $3\sigma$  LEVEL.

Name	RA (1950)	Dec (1950)	Line	$T_R^*$ , K	$V_{\text{LSR}}$ , km s $^{-1}$	$\Delta V$ , km s $^{-1}$
W3(3)	02 22 06.1	+61 50 40	1	0.19(0.01)	-39.31(0.11)	4.00(0.00)
			2	0.14(0.01)	-39.31(0.11)	4.00(0.00)
			3	0.10(0.01)	-39.31(0.11)	4.00(0.00)
			4	0.12(0.01)	-39.10(0.14)	4.00(0.34)
			5	0.09(0.01)	-38.50(0.18)	4.16(0.43)
W3(OH)	02 23 17.3	+61 38 58	1	0.60(0.01)	-46.56(0.04)	4.93(0.05)
			2	0.77(0.01)	-46.56(0.04)	4.93(0.05)
			3	0.73(0.01)	-46.56(0.04)	4.93(0.05)
			4	0.73(0.01)	-46.48(0.05)	5.53(0.11)
				0.32(0.03)	-43.12(0.04)	0.87(0.09)
			5	0.66(0.01)	-47.03(0.07)	5.20(0.00)
				0.39(0.02)	-43.31(0.01)	1.95(0.00)
			6	0.56(0.01)	-45.55(0.08)	7.34(0.11)
			7	0.47(0.02)	-46.03(0.25)	4.77(0.11)
				0.86(0.04)	-43.12(0.08)	0.49(0.03)
				0.41(0.01)	-45.87(0.08)	5.40(0.17)
				0.49(0.02)	-43.05(0.02)	0.90(0.06)
	0.06(0.01)	-45.44(0.37)	6.77(0.87)			
	0.11(0.004)	-45.71(0.09)	4.85(0.21)			
	0.45(0.01)	-46.53(0.05)	4.03(0.11)			
	0.66(0.02)	-46.57(0.05)	6.58(0.14)			
	0.17(0.02)	-46.04(0.08)	1.24(0.25)			
174.20-0.08	05 27 32.2	+33 45 52	1	0.21(0.01)	-2.91(0.10)	4.20(0.21)
			2	0.13(0.01)	-2.91(0.10)	4.20(0.21)
			3	0.08(0.01)	-2.91(0.10)	4.20(0.21)
			4	0.06(0.01)	-2.24(0.65)	5.74(1.52)
			5	<0.05		
Ori-S6	05 32 44.8	-05 26 00	1	1.28(0.03)	6.67(0.03)	4.04(0.05)
			2	1.58(0.02)	6.67(0.03)	4.04(0.05)
			3	1.48(0.04)	6.67(0.03)	4.04(0.05)
			4	1.44(0.13)	6.67(0.02)	4.02(0.01)
			5	1.20(0.13)	6.55(0.02)	4.06(0.01)
Ori-KL	05 32 47.0	-05 24 23	1	3.97(0.17)	8.11(0.06)	4.95(0.09)
			2	5.56(0.13)	8.11(0.06)	4.95(0.09)
			3	4.79(0.17)	8.11(0.06)	4.95(0.09)
			4	4.02(0.06)	8.08(0.04)	3.07(0.05)
				2.06(0.05)	7.09(0.05)	9.45(0.16)
			5	4.35(0.05)	7.94(0.04)	3.32(0.05)
				2.00(0.05)	6.95(0.06)	11.44(0.18)
			6	3.39(0.28)	8.16(0.12)	5.54(0.30)
				1.19(0.27)	6.11(0.62)	12.84(1.18)
			9	0.54(0.03)	8.43(0.03)	2.45(0.11)
				0.45(0.03)	8.11(0.06)	6.49(0.21)
10	0.95(0.03)	8.22(0.03)	2.41(0.09)			
	0.67(0.06)	7.62(0.06)	8.03(0.20)			
	1.37(0.05)	10.14(0.06)	1.93(0.10)			
	2.76(0.05)	8.17(0.03)	2.08(0.05)			
	0.92(0.03)	7.59(0.07)	7.99(0.16)			
OMC-2	05 32 59.8	-05 11 29	1	0.33(0.01)	11.23(0.04)	2.56(0.08)

TABLE 2—*Continued*

Name	RA (1950)	Dec (1950)	Line	$T_R^*$ , K	$V_{\text{LSR}}$ , km s $^{-1}$	$\Delta V$ , km s $^{-1}$
			2	0.36(0.01)	11.23(0.04)	2.56(0.08)
			3	0.34(0.01)	11.23(0.04)	2.56(0.08)
			4	0.27(0.01)	11.46(0.06)	2.85(0.16)
			5	0.20(0.01)	11.42(0.11)	4.14(0.26)
			9	<0.06		
			10	<0.09		
			11	0.22(0.03)	11.65(0.01)	2.50(0.19)
				1.04(0.03)	11.38(0.01)	0.69(0.02)
S231	05 35 51.3	+35 44 16	1	0.60(0.02)	-16.36(0.05)	3.61(0.09)
			2	0.50(0.02)	-16.36(0.05)	3.61(0.09)
			3	0.33(0.02)	-16.36(0.05)	3.61(0.09)
			4	0.34(0.04)	-16.08(0.22)	3.56(0.51)
			5	0.25(0.04)	-16.06(0.29)	3.44(0.69)
			6	0.13(0.01)	-16.07(0.04)	5.39(0.38)
			9	<0.06		
			10	<0.09		
			11	0.26(0.01)	-16.54(0.06)	2.82(0.13)
S235	05 37 31.8	+35 40 18	1	0.59(0.02)	-17.12(0.04)	2.52(0.07)
			2	0.62(0.02)	-17.12(0.04)	2.52(0.07)
			3	0.60(0.03)	-17.12(0.04)	2.52(0.07)
			4	0.45(0.02)	-17.01(0.06)	2.41(0.15)
			5	0.33(0.02)	-17.11(0.09)	2.59(0.21)
			9	<0.06		
			10	<0.09		
			11	0.65(0.01)	-16.79(0.02)	2.01(0.05)
NGC2071	05 44 30.0	+00 20 40	9	<0.09		
			10	<0.06		
			11	0.43(0.01)	9.68(0.04)	2.90(0.10)
Mon R2	06 05 20.0	-06 22 40	1	0.15(0.01)	10.36(0.08)	2.93(0.16)
			2	0.15(0.01)	10.36(0.08)	2.93(0.16)
			3	0.12(0.01)	10.36(0.08)	2.93(0.16)
			4	0.09(0.01)	10.90(0.13)	1.75(0.31)
			5	0.06(0.01)	10.70(0.32)	5.16(0.75)
			9	0.05(0.01)	9.67(0.32)	3.01(0.76)
			10	<0.09		
			11	0.10(0.02)	10.23(0.12)	2.07(0.28)
S252A	06 05 36.5	+20 39 34	1	0.30(0.01)	9.06(0.04)	2.61(0.08)
			2	0.27(0.01)	9.06(0.04)	2.61(0.08)
			3	0.22(0.01)	9.06(0.04)	2.61(0.08)
			4	0.12(0.01)	9.13(0.11)	1.95(0.27)
			5	0.13(0.02)	8.91(0.10)	1.72(0.24)
			9	<0.09		
			10	<0.09		
			11	0.08(0.01)	9.66(0.23)	3.25(0.52)
S252	06 05 53.7	+21 39 09	1	0.55(0.02)	3.17(0.04)	3.28(0.07)
			2	0.51(0.01)	3.17(0.04)	3.28(0.08)
			3	0.36(0.02)	3.17(0.04)	3.28(0.08)
			4	0.32(0.01)	3.35(0.05)	2.93(0.11)

TABLE 2—*Continued*

Name	RA (1950)	Dec (1950)	Line	$T_R^*$ , K	$V_{\text{LSR}}$ , km s $^{-1}$	$\Delta V$ , km s $^{-1}$
			5	0.12(0.06) 0.18(0.01) 0.09(0.06)	10.98(0.39) 3.05(0.07) 11.02(0.54)	1.64(0.91) 2.35(0.18) 1.83(1.26)
			9	<0.06		
			10	<0.09		
			11	0.24(0.01)	3.26(0.05)	2.76(0.11)
S255	06 10 01.0	+18 00 44	9	<0.06		
			10	<0.09		
			11	0.04(0.01)	8.40(0.43)	4.76(1.01)
S269 <sup>a</sup>	06 11 46.5	+13 50 39	1,2,3	0.14(0.02)	21.66(0.01)	1.40(0.23)
			4,5	<0.08		
			9	<0.12		
			10	<0.06		
			11	<0.02		
NGC 2264	06 38 24.9	+09 32 28	1	0.58(0.02)	7.82(0.05)	3.79(0.11)
			2	0.50(0.02)	7.82(0.05)	3.79(0.11)
			3	0.35(0.03)	7.82(0.05)	3.79(0.11)
			4	0.27(0.02)	7.98(0.09)	3.09(0.21)
			5	0.20(0.02)	7.42(0.12)	3.05(0.29)
			9	<0.06		
			10	<0.09		
			11	0.50(0.02)	7.93(0.04)	3.72(0.10)
				0.32(0.02)	7.54(0.03)	0.80(0.08)
NGC 2264G	06 38 28.0	+09 32 12	1	0.38(0.03)	7.74(0.09)	2.92(0.18)
			2	0.31(0.03)	7.74(0.09)	2.92(0.18)
			3	0.27(0.03)	7.74(0.09)	2.92(0.18)
			4	0.22(0.01)	8.08(0.20)	2.43(0.47)
			5	<0.2		
06446+0029	06 44 38.6	+00 29 26	9	<0.10		
			10	<0.10		
			11	<0.09		
345.01+1.79	16 53 19.7	-40 09 46	1	0.88(0.04)	-14.29(0.07)	4.86(0.14)
			2	0.98(0.03)	-14.29(0.07)	5.04(0.14)
			3	0.62(0.04)	-14.29(0.07)	5.04(0.14)
			4	0.64(0.08)	-13.83(0.32)	5.04(0.76)
				1.31(0.15)	-21.80(0.09)	1.64(0.21)
			5	0.58(0.03)	-14.00(0.12)	4.44(0.27)
				1.55(0.05)	-21.84(0.06)	1.72(0.06)
			6	0.43(0.03)	-13.70(0.08)	6.64(0.47)
				1.49(0.05)	-21.90(0.04)	1.70(0.07)
			7	0.35(0.02)	-13.39(0.20)	5.03(0.19)
				1.40(0.05)	-21.77(0.03)	1.62(0.06)
			8	0.28(0.02)	-13.46(0.03)	4.94(0.13)
				1.57(0.04)	-21.74(0.03)	1.90(0.05)
			9	<0.09		
			10	0.08(0.01)	-13.04(0.26)	4.18(0.62)
			11	1.89(0.02)	-13.90(0.02)	3.84(0.05)
			12	0.29(0.02)	-13.42(0.14)	3.47(0.34)

TABLE 2—*Continued*

Name	RA (1950)	Dec (1950)	Line	$T_R^*$ , K	$V_{\text{lsr}}$ , km s $^{-1}$	$\Delta V$ , km s $^{-1}$
345.51+0.35	17 00 53.4	−40 40 14	1	0.45(0.02)	−17.59(0.06)	5.11(0.10)
			2	0.55(0.01)	−17.59(0.06)	5.11(0.10)
			3	0.42(0.02)	−17.59(0.06)	5.11(0.10)
			4	0.43(0.01)	−17.56(0.06)	5.39(0.15)
			5	0.34(0.01)	−17.24(0.08)	5.22(0.19)
346.48+0.13 <sup>a</sup>	17 04 55.0	−40 01 40	1,2,3	0.05(0.01)	−8.7(0.9)	17.6(2.3)
NGC 6334B	17 16 34.5	−35 54 44	4,5	<0.06		
			1	0.97(0.02)	−6.78(0.03)	4.03(0.06)
			2	0.98(0.02)	−6.78(0.03)	4.03(0.06)
			3	0.74(0.02)	−6.78(0.03)	4.03(0.06)
			4	0.64(0.01)	−6.59(0.04)	3.89(0.09)
NGC 6334C	17 16 54.5	−35 51 58	5	0.46(0.01)	−6.65(0.06)	4.08(0.14)
			1	0.35(0.02)	−4.09(0.07)	3.59(0.13)
			2	0.41(0.02)	−4.09(0.07)	3.59(0.13)
			3	0.34(0.02)	−4.09(0.07)	3.59(0.13)
			4	0.24(0.01)	−4.24(0.08)	2.76(0.20)
NGC 6334F	17 17 32.3	−35 44 04	5	0.12(0.01)	−4.53(0.20)	3.61(0.48)
			1	1.75(0.03)	−7.74(0.03)	5.34(0.06)
			2	1.95(0.03)	−7.74(0.03)	5.34(0.06)
			3	1.61(0.04)	−7.74(0.03)	5.34(0.06)
			4	1.83(0.02)	−7.80(0.02)	5.67(0.05)
			5	1.67(0.02)	−8.01(0.03)	5.61(0.06)
			9	0.47(0.01)	−7.42(0.07)	7.32(0.16)
			10	0.52(0.01)	−7.95(0.04)	5.04(0.09)
			11	1.94(0.02)	−7.60(0.03)	5.00(0.04)
				0.45(0.03)	−9.15(0.04)	1.52(0.12)
				1.21(0.02)	−7.83(0.04)	5.96(0.11)
			351.78−0.54	17 23 20.9	−36 06 46	1
2	1.60(0.03)	−3.47(0.06)				7.88(0.11)
3	0.56(0.06)	−3.47(0.06)				7.88(0.11)
4	1.41(0.01)	−3.14(0.04)				8.59(0.09)
5	1.24(0.01)	−3.42(0.04)				8.70(0.11)
354.61+0.48	17 27 00.0	−33 11 38	1	0.15(0.01)	−20.24(0.10)	7.81(0.16)
			2	0.13(0.01)	−20.24(0.10)	7.81(0.16)
			3	0.07(0.01)	−20.24(0.10)	7.81(0.16)
			4	0.10(0.02)	−20.03(0.09)	7.35(0.21)
			5	0.09(0.02)	−20.01(0.10)	7.55(0.24)
353.41−0.36	17 27 06.6	−34 39 20	1	0.24(0.01)	−17.41(0.16)	6.87(0.29)
			2	0.17(0.01)	−17.41(0.16)	6.87(0.29)
			3	0.05(0.02)	−17.41(0.16)	6.87(0.29)
			4	0.10(0.01)	−16.94(0.37)	8.89(0.87)
			5	0.08(0.01)	−16.39(0.38)	5.46(0.90)
353.64−1.09 <sup>a</sup>	17 27 58.8	−35 41 56	1,2,3	0.07(0.01)	3.53(0.31)	5.24(0.73)
Sgr B2	17 44 10.7	−28 22 17	4,5	<0.07		
			1	−0.25(1.96)	54.32(4.89)	13.08(4.63)
			2	1.42(1.11)	54.32(4.89)	13.08(4.63)
			3	−0.32(3.32)	54.32(4.89)	13.08(4.63)
			4	1.27(0.05)	56.99(0.39)	21.33(0.93)

TABLE 2—*Continued*

Name	RA (1950)	Dec (1950)	Line	$T_R^*$ , K	$V_{\text{LSR}}$ , km s $^{-1}$	$\Delta V$ , km s $^{-1}$
0.54–0.86	17 47 04.1	–28 54 01	5	1.41(0.05)	59.56(0.31)	16.81(0.74)
			12	0.89(0.01)	60.81(0.07)	13.82(0.13)
			1	1.13(0.01)	16.60(0.03)	4.97(0.05)
			2	1.10(0.01)	16.60(0.03)	4.97(0.05)
			3	0.81(0.02)	16.60(0.03)	4.97(0.05)
			4	0.73(0.01)	16.94(0.04)	4.94(0.09)
			5	0.58(0.01)	16.84(0.05)	5.20(0.12)
			9	0.09(0.01)	16.48(0.24)	6.39(0.55)
			10	0.10(0.01)	17.95(0.23)	4.83(0.53)
			11	1.06(0.01)	17.12(0.04)	5.49(0.10)
			2.14+0.01	17 47 29.0	–27 05 01	1
2	0.09(0.01)	61.74(0.17)				5.49(0.26)
3	0.07(0.01)	61.74(0.17)				5.49(0.26)
4	0.09(0.01)	61.50(0.17)				5.59(0.42)
5	0.04(0.01)	61.70(0.75)				9.84(0.68)
2.55+0.18 <sup>a</sup>	17 47 44.4	–26 38 52	1,2,3	0.04(0.01)	8.37(0.83)	16.32(2.01)
			4,5	<0.05		
M8E	18 01 49.7	–24 26 56	1	0.50(0.03)	10.35(0.05)	1.90(0.07)
			2	0.38(0.03)	10.35(0.05)	1.90(0.07)
			3	0.39(0.03)	10.35(0.05)	1.90(0.07)
			4	0.23(0.02)	10.89(0.13)	2.41(0.30)
			5	0.15(0.02)	10.66(0.02)	2.61(0.49)
			9	<0.09		
			10	<0.12		
			11	0.37(0.04)	10.62(0.06)	2.68(0.16)
				1.56(0.04)	10.92(0.01)	0.78(0.02)
				0.39(0.02)	4.05(0.12)	5.66(0.17)
			9.62+0.19	18 03 16.0	–20 32 01	1
2	0.38(0.02)	4.05(0.12)				5.66(0.17)
3	0.32(0.03)	4.05(0.12)				5.66(0.17)
4	0.27(0.04)	2.95(0.21)				6.87(0.50)
5	0.23(0.02)	2.99(0.23)				6.29(0.55)
9	0.06(0.01)	4.44(0.23)				6.62(0.53)
10	0.07(0.01)	4.32(0.26)				7.63(0.61)
11	0.31(0.01)	4.14(0.05)				5.03(0.13)
1	0.29(0.02)	34.99(0.16)				5.78(0.22)
2	0.24(0.01)	34.99(0.16)				5.78(0.22)
8.67–0.36	18 04 55.0	–20 19 58				3
			4	0.24(0.01)	35.05(0.12)	4.65(0.29)
			5	0.19(0.01)	35.22(0.16)	4.81(0.37)
			6	0.15(0.02)	35.35(0.42)	5.17(0.72)
			1,2,3	0.05(0.01)	49.13(0.60)	10.22(1.48)
			4,5	<0.1		
9.98–0.04 <sup>a</sup>	18 04 55.0	–20 19 58	1	0.97(0.03)	66.43(0.09)	8.13(0.15)
			2	0.92(0.02)	66.43(0.09)	8.13(0.15)
			3	0.33(0.03)	66.43(0.09)	8.13(0.15)
			4	0.76(0.02)	66.35(0.10)	7.63(1.02)
			5	0.60(0.02)	65.99(0.14)	8.98(0.31)
			6	0.44(0.02)	66.39(0.33)	10.24(0.35)
W31(1)	18 05 40.5	–19 52 23	1	0.97(0.03)	66.43(0.09)	8.13(0.15)
			2	0.92(0.02)	66.43(0.09)	8.13(0.15)
			3	0.33(0.03)	66.43(0.09)	8.13(0.15)
			4	0.76(0.02)	66.35(0.10)	7.63(1.02)
			5	0.60(0.02)	65.99(0.14)	8.98(0.31)
			6	0.44(0.02)	66.39(0.33)	10.24(0.35)

TABLE 2—*Continued*

Name	RA (1950)	Dec (1950)	Line	$T_R^*$ , K	$V_{\text{LSR}}$ , km s <sup>-1</sup>	$\Delta V$ , km s <sup>-1</sup>
10.30–0.15	18 05 57.9	–20 06 26	9	0.21(0.01)	66.86(0.08)	9.60(0.18)
			10	0.25(0.01)	66.50(0.09)	9.90(0.21)
			11	0.75(0.01)	66.40(0.04)	8.75(0.10)
			1	0.19(0.02)	13.16(0.20)	6.46(0.00)
			2	0.21(0.01)	13.16(0.20)	9.46(0.00)
			3	0.15(0.02)	13.16(0.20)	6.46(0.00)
W31C	18 07 30.5	–19 56 28	4	0.07(0.01)	12.44(0.37)	6.46(0.86)
			5	0.06(0.01)	11.25(0.31)	3.20(0.73)
			1	0.57(0.02)	–3.56(0.06)	6.79(0.09)
			2	0.64(0.01)	–3.56(0.06)	6.79(0.09)
			3	0.47(0.02)	–3.56(0.06)	6.79(0.09)
			4	0.51(0.01)	–3.33(0.06)	7.53(0.16)
			5	0.39(0.01)	–3.31(0.09)	7.99(0.22)
			6	0.22(0.02)	–2.86(0.49)	8.94(0.42)
			9	0.04(0.01)	–2.10(0.48)	6.36(1.14)
			10	0.05(0.01)	–3.95(0.26)	3.11(0.60)
			11 <sup>c</sup>	0.16(0.02)	1.58(0.22)	3.03(0.35)
12.89+0.49	18 08 56.4	–17 32 14		0.76(0.01)	–2.67(0.06)	4.86(0.37)
				0.06(0.01)	–6.38(0.08)	0.62(0.23)
				0.40(0.03)	–7.09(0.16)	3.54(0.18)
			1	0.43(0.01)	32.71(0.05)	3.98(0.09)
			2	0.42(0.01)	32.71(0.05)	3.98(0.09)
			3	0.32(0.02)	32.71(0.05)	3.98(0.09)
11.91–0.15 <sup>a</sup>	18 09 18.1	–18 42 25	4	0.30(0.03)	32.88(0.23)	4.27(0.54)
			5	0.26(0.03)	33.02(0.28)	4.76(0.67)
			1,2,3	0.07(0.01)	41.39(0.49)	5.58(1.15)
			4,5	<0.1		
			1	0.35(0.02)	22.94(0.16)	9.20(0.25)
12.22–0.12	18 09 45.0	–18 25 10	2	0.27(0.01)	22.94(0.16)	9.20(0.25)
			3	0.07(0.02)	22.94(0.16)	9.20(0.25)
			4	0.20(0.01)	23.83(0.20)	8.12(0.48)
			5	0.16(0.01)	23.57(0.27)	8.92(0.64)
			6	0.13(0.01)	23.07(0.05)	11.12(0.53)
			W33B	18 10 59.3	–18 02 40	1
2	0.23(0.01)	55.24(0.12)				6.05(0.00)
3	0.17(0.01)	55.24(0.12)				6.05(0.00)
4	0.12(0.01)	55.99(0.15)				6.12(0.35)
5	0.15(0.01)	56.14(0.12)				5.99(0.28)
6	0.08(0.01)	56.34(0.36)				7.41(0.35)
11.94–0.62	18 11 04.4	–18 54 20	1	0.35(0.01)	38.23(0.06)	4.19(0.09)
			2	0.31(0.01)	38.23(0.06)	4.19(0.09)
			3	0.24(0.01)	38.23(0.06)	4.19(0.09)
			4	0.16(0.01)	38.42(0.09)	3.42(0.22)
			5	0.09(0.01)	38.16(0.20)	5.13(0.48)
W33Met	18 11 15.7	–17 56 53	1	0.50(0.02)	36.40(0.06)	4.62(0.09)
			2	0.52(0.01)	36.40(0.06)	4.62(0.09)
			3	0.44(0.02)	36.40(0.06)	4.62(0.09)
			4	0.28(0.01)	36.28(0.06)	4.56(0.16)

TABLE 2—*Continued*

Name	RA (1950)	Dec (1950)	Line	$T_{R}^*$ , K	$V_{\text{LSR}}$ , km s $^{-1}$	$\Delta V$ , km s $^{-1}$
			5	0.18(0.01)	36.56(0.10)	4.34(0.24)
			6	0.07(0.01)	35.92(0.05)	5.96(0.28)
			9	<0.06		
			10	<0.08		
			11	0.67(0.01)	36.75(0.02)	3.57(0.06)
				0.43(0.02)	32.78(0.02)	1.03(0.05)
W33A <sup>a</sup>	18 11 44.2	−17 52 58	1,2,3	0.32(0.02)	37.30(0.53)	14.29(1.26)
			4,5	<0.3		
GGD 27	18 16 13.8	−20 48 31	1	0.40(0.02)	12.61(0.05)	2.40(0.10)
			2	0.32(0.02)	12.61(0.05)	2.40(0.10)
			3	0.14(0.02)	12.61(0.05)	2.40(0.10)
			4	0.13(0.03)	13.11(0.33)	3.42(0.77)
			5	0.12(0.03)	11.96(0.30)	2.21(0.70)
			9	<0.06		
			10	<0.08		
			11	0.39(0.01)	13.04(0.03)	1.59(0.06)
M17	18 17 31.8	−16 13 00	1	0.16(0.01)	19.44(0.06)	4.23(0.10)
			2	0.26(0.01)	19.44(0.06)	4.23(0.10)
			3	0.24(0.01)	19.44(0.06)	4.23(0.10)
			4	0.20(0.01)	19.32(0.09)	4.58(0.23)
			5	0.14(0.01)	19.39(0.16)	5.59(0.38)
			6	0.09(0.01)	19.87(0.50)	5.58(0.40)
L379	18 26 32.9	−15 17 51	1	0.34(0.02)	18.30(0.21)	8.03(0.32)
			2	0.28(0.02)	18.30(0.21)	8.03(0.32)
			3	0.14(0.03)	18.30(0.21)	8.03(0.32)
			4	0.29(0.01)	17.97(0.14)	5.99(0.33)
			5	0.17(0.01)	17.61(0.26)	7.29(0.62)
			9	<0.06		
			10	<0.09		
			11 <sup>c</sup>	1.19(0.02)	20.12(0.04)	2.21(0.07)
				0.90(0.02)	17.78(0.05)	2.19(0.09)
				0.56(0.02)	17.60(0.08)	10.61(0.20)
23.43−0.19	18 31 55.8	−08 34 17	1	0.33(0.01)	101.29(0.12)	7.57(0.00)
			2	0.22(0.01)	101.29(0.12)	7.57(0.00)
			3	0.05(0.02)	101.29(0.12)	7.57(0.00)
			4	0.14(0.01)	101.18(0.17)	7.57(0.40)
			5	0.09(0.01)	100.38(0.31)	10.67(0.74)
23.01−0.41	18 31 56.7	−09 03 18	1	0.30(0.01)	76.48(0.15)	8.90(0.23)
			2	0.19(0.01)	76.48(0.15)	8.90(0.23)
			3	0.03(0.02)	76.48(0.15)	8.90(0.23)
			4	0.11(0.01)	77.18(0.17)	7.42(0.39)
			5	0.10(0.01)	77.15(0.17)	7.46(0.40)
W42	18 33 30.6	−07 15 07	1	0.35(0.01)	110.29(0.11)	6.33(0.18)
			2	0.29(0.01)	110.29(0.11)	6.33(0.18)
			3	0.12(0.02)	110.29(0.11)	6.33(0.18)
			4	0.18(0.01)	111.20(0.14)	7.72(0.32)
			5	0.16(0.01)	111.29(0.15)	6.33(0.35)
			6	0.18(0.01)	110.51(0.32)	8.62(0.74)



TABLE 2—*Continued*

Name	RA (1950)	Dec (1950)	Line	$T_{R}^*$ , K	$V_{\text{LSR}}$ , km s $^{-1}$	$\Delta V$ , km s $^{-1}$			
18379–0546	18 37 57.4	–05 46 10	9	<0.11					
			10	<0.12					
			11	<0.09					
29.95–0.02	18 43 27.1	–02 42 36	1	0.33(0.01)	97.77(0.07)	4.71(0.11)			
			2	0.38(0.01)	97.77(0.07)	4.71(0.11)			
			3	0.31(0.01)	97.77(0.07)	4.71(0.11)			
			4	0.26(0.01)	97.64(0.06)	4.06(0.16)			
			5	0.21(0.01)	98.12(0.08)	4.40(0.20)			
30.70–0.06	18 44 58.9	–02 04 27	1	0.31(0.01)	91.21(0.08)	5.15(0.13)			
			2	0.22(0.01)	91.21(0.08)	5.15(0.13)			
			3	0.15(0.02)	91.21(0.08)	5.15(0.13)			
			4	0.10(0.01)	91.14(0.22)	4.47(0.51)			
			5	0.09(0.01)	91.06(0.25)	4.76(0.60)			
34.26+0.15	18 50 46.2	+01 11 12	1	0.97(0.02)	57.83(0.04)	5.90(0.06)			
			2	1.11(0.02)	57.83(0.04)	5.90(0.06)			
			3	0.95(0.03)	57.83(0.04)	5.90(0.06)			
			4	0.92(0.01)	58.16(0.04)	6.26(0.08)			
			5	0.78(0.01)	58.09(0.04)	6.59(0.11)			
			6	0.56(0.01)	58.43(0.12)	7.77(0.14)			
			9	0.26(0.01)	59.04(0.06)	6.33(0.14)			
			10	0.25(0.01)	58.99(0.07)	6.88(0.16)			
			11	1.64(0.01)	58.79(0.01)	5.60(0.03)			
			35.03+0.35	18 51 30.3	+01 57 30	1	0.16(0.01)	52.99(0.09)	4.07(0.16)
						2	0.18(0.01)	52.99(0.09)	4.07(0.16)
3	0.11(0.01)	52.99(0.09)				4.07(0.16)			
4	0.07(0.01)	52.61(0.22)				2.67(0.52)			
5	0.05(0.01)	53.11(0.42)				5.03(0.99)			
35.19–0.74	18 55 40.8	+01 36 30	1	0.50(0.03)	34.10(0.11)	5.79(0.15)			
			2	0.51(0.02)	34.10(0.11)	5.79(0.15)			
			3	0.46(0.03)	34.10(0.11)	5.79(0.15)			
			4	0.38(0.01)	34.37(0.12)	6.90(0.28)			
			5	0.37(0.01)	33.55(0.12)	6.60(0.28)			
			6	0.18(0.02)	32.96(0.55)	8.31(0.43)			
			9	0.06(0.01)	31.70(0.28)	7.16(0.65)			
			10	0.06(0.01)	31.18(0.20)	3.32(0.46)			
			11	1.07(0.01)	34.22(0.02)	4.18(0.05)			
			W48	18 59 13.8	+01 09 20	1	0.18(0.04)	42.10(0.08)	3.44(0.00)
							0.05(0.01)	45.70(0.08)	2.09(0.00)
2	0.14(0.01)	42.10(0.08)				3.44(0.00)			
	0.16(0.01)	45.70(0.08)				2.09(0.00)			
3	0.11(0.01)	42.10(0.08)				3.44(0.00)			
	0.11(0.05)	45.70(0.08)				2.09(0.00)			
4	0.16(0.02)	41.69(0.22)				3.75(0.52)			
	0.38(0.03)	45.47(0.07)				2.52(0.15)			
5	0.14(0.02)	41.67(0.17)				3.13(0.44)			
	0.46(0.03)	45.34(0.08)				1.95(0.05)			
6	0.11(0.01)	41.34(0.08)				3.00(0.05)			
	0.36(0.01)	45.05(0.03)				1.89(0.05)			

TABLE 2—*Continued*

Name	RA (1950)	Dec (1950)	Line	$T_{R}^*$ , K	$V_{\text{LSR}}$ , km s $^{-1}$	$\Delta V$ , km s $^{-1}$
W49N	19 07 49.9	+09 01 14	7	0.12(0.01)	41.75(0.82)	3.71(0.20)
				0.39(0.02)	45.18(0.15)	1.37(0.07)
			8	0.15(0.01)	41.66(0.16)	2.80(0.41)
				0.31(0.03)	45.39(0.07)	2.05(0.15)
			9	<0.05		
			10	<0.12		
			11	0.07(0.01)	43.55(0.23)	2.91(0.55)
			12	0.09(0.01)	42.64(0.15)	4.46(0.36)
			1	0.03(0.10)	10.47(1.48)	15.45(1.31)
			2	0.48(0.09)	10.47(1.48)	15.45(1.31)
			3	0.29(0.08)	10.47(1.48)	15.45(1.31)
4	0.30(0.01)	7.77(0.13)	13.35(0.32)			
5	0.28(0.01)	8.08(0.16)	16.21(0.37)			
6	0.20(0.01)	7.06(0.44)	14.04(1.04)			
9	<0.07					
10	0.23(0.01)	10.03(0.12)	16.61(0.29)			
11 <sup>c</sup>	0.09(0.01)	18.34(1.29)	9.06(1.81)			
	0.49(0.03)	12.51(0.09)	5.44(0.23)			
	0.30(0.01)	4.93(0.14)	7.82(0.29)			
43.80–0.13	19 09 30.8	+09 30 47	1	0.27(0.01)	43.22(0.11)	6.62(0.18)
			2	0.19(0.01)	43.22(0.11)	6.62(0.18)
			3	0.08(0.01)	43.22(0.11)	6.62(0.18)
			4	0.12(0.01)	43.93(0.20)	7.39(0.47)
			5	0.09(0.01)	42.99(0.25)	6.77(0.60)
			6	0.08(0.01)	42.54(0.45)	7.48(0.46)
W51	19 21 24.4	+14 24 48	1	0.51(0.02)	59.54(0.09)	8.25(0.14)
			2	0.51(0.01)	59.54(0.09)	8.25(0.14)
			3	0.24(0.02)	59.54(0.09)	8.25(0.14)
			4	0.34(0.01)	59.07(0.10)	10.26(0.23)
			5	0.24(0.01)	58.63(0.13)	8.55(0.29)
			6	0.20(0.01)	57.85(0.33)	9.93(0.36)
W51E1/E2	19 21 26.2	+14 24 43	1	1.81(0.03)	55.95(0.05)	8.63(0.07)
			2	1.81(0.02)	55.95(0.05)	8.63(0.07)
			3	0.91(0.03)	55.95(0.05)	8.63(0.07)
			4	1.65(0.01)	56.19(0.03)	8.74(0.06)
			5	1.42(0.01)	56.05(0.03)	8.33(0.07)
			9	0.41(0.01)	56.04(0.07)	7.96(0.16)
W51Met1	19 21 26.2	+14 23 32	10	0.44(0.01)	56.63(0.09)	9.56(0.20)
			11	2.74(0.02)	56.05(0.02)	7.11(0.05)
			1	0.36(0.03)	55.10(0.20)	6.54(0.29)
			2	0.28(0.02)	55.10(0.20)	6.54(0.29)
			3	0.22(0.03)	55.10(0.20)	6.54(0.29)
			4	0.19(0.01)	55.69(0.25)	7.95(0.59)
W51Met3	19 21 27.5	+14 23 52	5	0.12(0.01)	57.68(0.44)	9.29(1.04)
			10	<0.08		
			11	0.10(0.01)	55.23(0.21)	4.26(0.50)
			1	0.50(0.02)	54.37(0.10)	5.33(0.15)
			2	0.39(0.01)	54.37(0.10)	5.33(0.15)

TABLE 2—*Continued*

Name	RA (1950)	Dec (1950)	Line	$T_R^*$ , K	$V_{\text{LSR}}$ , km s $^{-1}$	$\Delta V$ , km s $^{-1}$
W51Met2	19 21 28.8	+14 23 47	3	0.30(0.03)	54.37(0.10)	5.33(0.15)
			4	0.23(0.01)	54.98(0.19)	6.97(0.44)
			5	0.16(0.01)	54.56(0.23)	5.39(0.54)
			1	0.50(0.02)	55.20(0.09)	5.20(0.12)
			2	0.53(0.02)	55.20(0.09)	5.20(0.12)
19410+2336	19 41 04.2	+23 36 42	3	0.50(0.03)	55.20(0.09)	5.20(0.12)
			4	0.34(0.02)	55.17(0.13)	5.19(0.31)
			5	0.24(0.02)	55.24(0.18)	4.74(0.43)
			1	0.30(0.01)	22.55(0.05)	2.73(0.09)
			2	0.24(0.01)	22.55(0.05)	2.73(0.09)
ON1	20 08 10.0	+31 22 40	3	0.20(0.01)	22.55(0.05)	2.73(0.09)
			4	0.14(0.01)	22.67(0.12)	3.45(0.29)
			5	0.07(0.01)	22.53(0.28)	4.30(0.66)
			9	<0.06		
			10	<0.06		
ON2	20 19 50.0	+37 16 30	11	0.47(0.01)	22.72(0.02)	2.31(0.06)
			1	0.43(0.01)	11.73(0.03)	3.82(0.06)
			2	0.36(0.01)	11.73(0.03)	3.82(0.06)
			3	0.26(0.01)	11.73(0.03)	3.82(0.06)
			4	0.22(0.01)	12.16(0.08)	4.49(0.19)
W75N	20 36 50.4	+42 27 23	5	0.14(0.01)	11.57(0.13)	4.88(0.31)
			9	<0.09		
			10	<0.06		
			11	0.36(0.02)	11.51(0.05)	4.55(0.15)
			1	0.02(0.01)	0.01(0.24)	3.51(0.47)
DR21West	20 37 07.6	+42 08 46	2	0.05(0.01)	0.01(0.24)	3.51(0.47)
			3	0.08(0.01)	0.01(0.24)	3.51(0.47)
			4	0.07(0.01)	−0.31(0.21)	2.18(0.49)
			5	<0.06		
			1	0.48(0.01)	8.96(0.05)	3.95(0.08)
DR21MetC	20 37 12.6	+42 08 46	2	0.45(0.01)	8.96(0.05)	3.95(0.08)
			3	0.33(0.02)	8.96(0.05)	3.95(0.08)
			4	0.31(0.01)	9.38(0.08)	4.24(0.18)
			5	0.25(0.01)	8.94(0.09)	4.16(0.22)
			9	0.06(0.01)	9.38(0.24)	5.56(0.57)
DR21MetC	20 37 12.6	+42 08 46	10	<0.06		
			11	0.63(0.01)	8.92(0.02)	3.68(0.05)
			1	0.14(0.01)	−3.55(0.15)	4.98(0.27)
			2	0.15(0.01)	−3.55(0.15)	4.98(0.27)
			3	0.08(0.01)	−3.55(0.15)	4.98(0.27)
DR21MetC	20 37 12.6	+42 08 46	4	0.11(0.01)	−3.39(0.23)	6.34(0.55)
			5	0.09(0.01)	−5.28(0.37)	10.92(0.88)
			9	<0.06		
			10	<0.07		
			11	1.82(0.02)	−2.48(0.01)	0.63(0.01)
DR21MetC	20 37 12.6	+42 08 46	1	0.32(0.01)	−2.77(0.06)	4.20(0.15)
			2	0.17(0.01)	−2.37(0.13)	4.40(0.20)
			2	0.19(0.01)	−2.37(0.13)	4.40(0.20)

TABLE 2—*Continued*

Name	RA (1950)	Dec (1950)	Line	$T_R^*$ , K	$V_{\text{LSR}}$ , km s $^{-1}$	$\Delta V$ , km s $^{-1}$
DR21OH	20 37 13.8	+42 12 13	3	0.17(0.01)	−2.37(0.13)	4.40(0.20)
			4	0.13(0.01)	−3.00(0.17)	5.91(0.41)
			5	0.08(0.01)	−2.92(0.26)	5.21(0.60)
			1	0.76(0.02)	−3.02(0.04)	5.24(0.06)
			2	0.86(0.01)	−3.02(0.04)	5.24(0.06)
			3	0.67(0.02)	−3.02(0.04)	5.24(0.06)
			4	0.69(0.01)	−2.74(0.03)	5.54(0.08)
			5	0.58(0.01)	−2.81(0.04)	6.11(0.09)
			9	0.06(0.01)	−2.80(0.19)	4.11(0.44)
			10	0.05(0.01)	−2.02(0.22)	4.52(0.51)
			11 <sup>c</sup>	1.91(0.09)	0.35(0.01)	0.83(0.07)
W75S(3)	20 37 16.7	+42 15 15		1.26(0.03)	−3.05(0.10)	5.09(0.12)
			1	0.31(0.01)	−4.14(0.08)	3.87(0.15)
			2	0.25(0.01)	−4.14(0.08)	3.87(0.15)
			3	0.20(0.02)	−4.14(0.08)	3.87(0.15)
			4	0.13(0.01)	−4.19(0.17)	3.97(0.40)
IC1396N <sup>a</sup>	21 39 10.3	58 02 29	5	0.16(0.01)	−3.95(0.12)	3.05(0.29)
			1,2,3	0.12(0.02)	−0.5(1.45)	19.84(3.43)
S140	22 17 41.2	+63 03 43	4,5	<0.09		
			1	0.32(0.01)	−6.93(0.04)	2.75(0.08)
			2	0.33(0.01)	−6.93(0.04)	2.75(0.08)
			3	0.31(0.01)	−6.93(0.04)	2.75(0.08)
			4	0.29(0.01)	−6.81(0.06)	2.46(0.14)
			5	0.19(0.01)	−7.31(0.09)	2.78(0.22)
			9	<0.05		
			10	<0.06		
			11	0.46(0.01)	−6.95(0.03)	2.29(0.06)
			Cep A <sup>b</sup>	22 54 19.2	+61 45 47	1
2	0.18(0.01)	−10.63(0.10)				3.91(0.17)
3	0.21(0.02)	−10.63(0.10)				3.91(0.17)
4	0.12(0.02)	−9.82(0.04)				4.89(0.69)
	0.56(0.03)	−2.41(0.05)				2.02(0.11)
5	0.16(0.01)	−9.45(0.68)				4.54(0.74)
	1.01(0.03)	−2.48(0.03)				2.17(0.08)
6	0.10(0.01)	−10.82(0.14)				4.46(0.06)
	1.11(0.01)	−2.53(0.02)				1.81(0.03)
7	0.09(0.01)	−10.85(0.16)				2.75(0.38)
	0.71(0.06)	−2.53(0.10)				2.28(0.23)
8	0.77(0.03)	−2.39(0.04)				1.93(0.11)
NGC7538	23 11 36.6	+61 11 50	9	<0.06		
			10	<0.09		
			11	0.17(0.01)	−10.31(0.08)	3.19(0.19)
			12	0.09(0.01)	−5.09(0.17)	4.49(0.43)
				0.13(0.01)	−10.63(0.10)	3.21(0.24)
			1	0.39(0.02)	−57.33(0.05)	4.13(0.09)
	0.42(0.01)	−57.33(0.05)	4.13(0.09)			
	0.44(0.02)	−57.33(0.05)	4.13(0.09)			

TABLE 2—*Continued*

Name	RA (1950)	Dec (1950)	Line	$T_R^*$ , K	$V_{\text{lsr}}$ , km s <sup>-1</sup>	$\Delta V$ , km s <sup>-1</sup>
			4	0.57(0.01)	-57.13(0.03)	4.71(0.07)
			5	0.50(0.01)	-57.20(0.03)	4.96(0.08)
			6	0.33(0.01)	-57.16(0.09)	6.10(0.10)
			9	0.05(0.01)	-58.70(0.22)	4.42(0.52)
			10	0.06(0.01)	-58.58(0.31)	3.99(0.42)
			11	0.57(0.01)	-57.43(0.02)	3.23(0.05)

<sup>a</sup>blends of the  $J = 1, 2,$  and  $3$  157 GHz components were fitted as single lines at a frequency of those of the  $J = 3$  line.

<sup>b</sup>narrow features consist of several components (see Slysh et al. 1995).

<sup>c</sup>a single asymmetric feature was fitted by several gaussians.

TABLE 5

Excitation temperatures of various methanol transitions derived from the 133, 157, and 166 GHz data. The rms errors in parenthesis take into account the fitting errors from Table 2 as well as calibration errors.

Source Name	$T_{\text{ex}}$ , K $5_{-2} - 6_{-1} E$	$T_{\text{ex}}$ , K $6_{-1} - 5_0 E$ unresolved/extended	$T_{\text{ex}}$ , K $5_0 - 4_0 E$	$T_{\text{ex}}$ , K $6_0 - 6_{-1} E$ unresolved/extended	$T_{\text{ex}}$ , K $7_1 - 7_0 E$ unresolved/extended
W3(3)			29(8)		
W3(OH)	14(1)	-23(12)/100(300) <sup>n</sup>	36(2)	24(2)/-255(239)	-53(62)/-32(23) <sup>n</sup>
174.20-0.08					
Ori-S6			31(1)		
Ori-KL	7(1)	-35(30)/42(36)	171(51)	20(2)/254(261)	
OMC-2	0-37	-11(4)/-29(30)	85(43)		
S231	0-19	-8(2)/-14(6)	21(2)	6.3(0.5)/8.8(0.8)	
S235	0-5	-10(3)/-23(15)	28(6)	7.1	
NGC2071	0-5				
Mon R2	< -10	-85(288)/24(24)			
S252A	< -8	-6(1)/-8(3)	46(30)		
S252	0-21	-5(1)/-6(1)	12(1)		
S255	< -4				
S269				4.2	
NGC2264	0-6	-3.0(1)/-4(1)	22(4)		
NGC2264G					
345.01+1.79	4(1)	-4(1)/-4.3(0.6)	29(4)	3.2(0.1)/3.8(0.1)	15(6)/19(10)
345.51+0.35			25(2)		
NGC6334-B			24(2)		
NGC6334-C			18(4)		
NGC6334-F	10(1)	-6.0(1)/-9(2)	38(2)		
351.78-0.54			37(2)		
354.61+0.48			44(6)		
353.41-0.36			12(2)		
Sgr B2			55(3)		
0.54-0.86	5(1)	-4(1)/-5(1)	30(2)		
2.14+0.01			65(44)		
2.55+0.18					
M8E	0-16	-3.5(0.6)/-4.1(0.6)	20(6)		
9.62+0.19	6(1)	-6(1)/-10(3)	27(6)		
8.67-0.36			31(7)		
W31(1)	25(2)	-6(1)/-9(2)	47(3)	4.9(0.2)/6.4(0.3)	
10.30-0.15			9(2)		
W31C	2(1)	-2.9(0.3)/-3.5(0.4)	27(2)	3.4(0.1)/4.0(0.2)	
12.89+0.49			47(7)		
11.91-0.15					
12.22-0.12			34(8)		
W33B			408(922)		
11.94-0.62			31(8)		
W33Met	0-9	-2.6(0.3)/-3.0(0.3)	17(1)	2.4(0.1)/2.7(0.1)	
W33A					
GGD27	0-9	-3.4(0.5)/-4.2(0.7)	15(4)		
M17			30(5)		
L379			22(3)		
23.43-0.19			14(1)		
23.01-0.41			52(15)		
W42			21(2)		
18379-0546					
29.95-0.02			37(6)		
30.70-0.06			44(25)		
34.26+0.15	7(1)	-4.2(0.5)/-5(1)	37(2)	4.0(0.1)/4.9(0.1)	
35.03+0.35					
35.19-0.74	3(1)	-4.0(0.5)/-5(1)	41(7)	5.4(0.5)/7.1(0.8)	
43.80-0.13			16(2)		
W51			18(3)		
W51E1/E2	6(1)	-4.4(0.6)/-6(1)	29(1)		
W51Met1		-254(2500)/21(14)	22(4)		
W51Met3			15(2)		
W51Met2			17(2)		
19410+2336	0-7	-2.8(0.4)/-3.3(0.5)	17(4)		
ON1	0-13	-3.5(0.3)/-4.2(0.5)	22(3)		
ON2					
W75N	5(1)	-3.7(0.3)/-4.6(0.8)	29(4)		
DR21West	0-12	-5(1)/-7(1)			
DR21MetC			15(2)		
DR21OH	3(1)	-3.7(0.5)/-4.5(0.6)	42(3)		
W75S(3)			32(10)		
S140	0-7	-3.9(0.5)/-5.0(0.8)	25(4)		
Cep A	< -75	-9(2)/-17(9)	28(9)	6.5(0.5)/9.2(1.0)	-19(10)/-15(6)
NGC7538	6(1)	-10(3)/-21(12)	44(3)	7.4(0.2)/11.2(0.4)	